ACS OMEGA

http://pubs.acs.org/journal/acsodf

Article

Differential Volatile Organic Compound Expression in the Interaction of *Daldinia eschscholtzii* and *Mycena citricolor*

Efraín Escudero-Leyva, Luis Quirós-Guerrero, Víctor Vásquez-Chaves, Reinaldo Pereira-Reyes, Priscila Chaverri, and Giselle Tamayo-Castillo*

Cite This: *ACS Omega* 2023, 8, 31373−31388

Read Online

ACCESS | Metrics & More | Article Recommendations | Supporting Information

ABSTRACT: Fungi exhibit a wide range of ecological guilds, but those that live within the inner tissues of plants (also known as endophytes) are particularly relevant due to the benefits they sometimes provide to their hosts, such as herbivory deterrence, disease protection, and growth promotion. Recently, endophytes have gained interest as potential biocontrol agents against crop pathogens, for example, coffee plants (*Coffea arabica*). Published results from research performed in our laboratory showed that endophytic fungi isolated from wild Rubiaceae plants were effective in reducing the effects of the American leaf spot of coffee (*Mycena citricolor*). One of these isolates (GU11N) from the plant *Randia grandifolia* was identified as *Daldinia eschscholtzii* (Xylariales). Its antagonism mechanisms, effects, and chemistry against *M. citricolor* were investigated by analyzing its volatile profile alone and in the presence of the pathogen in contactless and dual culture assays. The experimental design involved direct sampling of agar plugs in vials for headspace (HS) and headspace solid-phase microextraction (HS-SPME) gas chromatography-mass spectrometry (GC-MS) analysis. Additionally, we used ultrahigh-performance liquid chromatography coupled to high-resolution mass spectrometry (UHPLC-HRMS/MS) to identify nonvolatile compounds from organic extracts of the mycelia involved in the interaction. Results showed that more volatile compounds were identified using HS-SPME (39 components) than those by the HS technique (13 components), sharing only 12 compounds. Statistical tests suggest that *D. eschscholtzii* inhibited the growth of *M. citricolor* through the release of VOCs containing a combination of 1,8-dimethoxynapthhalene and terpene compounds affecting *M. citricolor* pseudopilei. The damaging effects of 1,8-dimethoxynaphthalene were corroborated in an in vitro test against *M. citricolor* pseudopilei; scanning electron microscopy (SEM) photographs confirmed structural damage. After analyzing the UHPLC-HRMS/MS data, a predominance of fatty acid derivatives was found among the putatively identified compounds. However, a considerable proportion of features (37.3%) remained unannotated. In conclusion, our study suggests that *D. eschscholtzii* has potential as a biocontrol agent against *M. citricolor* and that 1,8-dimethoxynaphthalene contributes to the observed damage to the pathogen's reproductive structures.

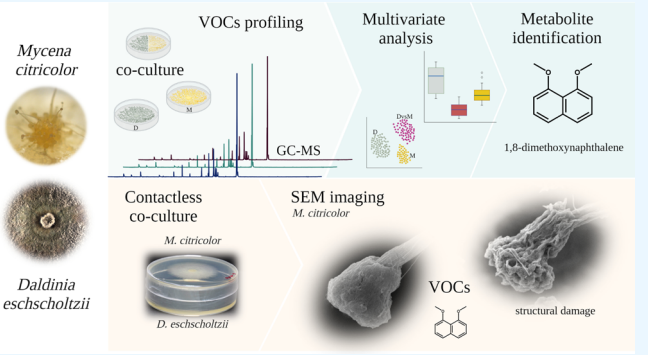

INTRODUCTION

Endophytic fungi are keystone microorganisms in the phytobiome, with a wide variety of symbiotic associations ranging from mutualism to parasitism.[1] Almost every plant on the planet has developed a symbiotic relationship (in the broad sense) with fungal endophytes and, in some cases, their presence translates to benefits.[2,3] Nowadays, several reports highlight the role of volatile organic compounds (VOCs) as a key factor in the fungal ecological interactions with other fungi, bacteria, and plants.[4] These VOCs are known to regulate growth in spores and seeds,[5] modify signaling for herbivore deterrence,[6] pathogen inhibition,[7] among other functions. The production of VOCs by fungi is influenced by numerous factors, including environmental conditions.[8]

Many studies have reported on the fungistatic or fungicidal effects of VOCs from endophytic fungi[9] (see some examples of compounds in Figure 1). Mycofumigation activity has been reported for 5-pentyl-2-furaldehyde (Figure 1.1) from *Irpex* (=*Oxyporus*) *latemarginatus*[10] and 6-pentyl-α-pyrone (6PP) (Figure 1.2) from endophytic *Trichoderma asperellum* IsmT5.[11] The latter induced the accumulation of compounds related to plant defense and increased the production of anthocyanins and trichomes in *Arabidopsis thaliana*. *Induratia kashay* (=*Muscodor kashay*), isolated from the medicinal plant *Aegle marmelos*, has been found to inhibit fungal pathogens such as *Alternaria*

Received: June 1, 2023
Accepted: July 31, 2023
Published: August 18, 2023

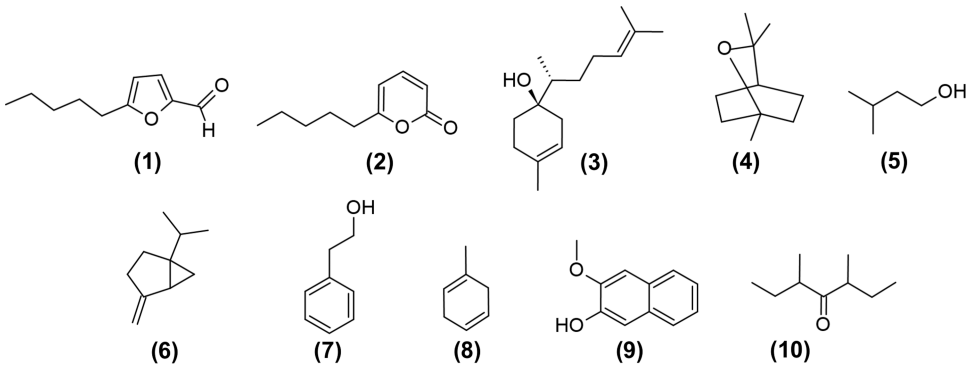

Figure 1. Examples of VOCs reported from several endophytic fungi.

alternata and *Aspergillus flavus* in contactless assays.[12] Among the 23 VOCs reported by Meshram et al.,[12] *β*-bisabolol (Figure 1.3) was identified as the major component. A *Hypoxylon* species recovered from the plant *Persea indica* was found to exhibit antagonistic activity against *Botrytis cinerea*, *Cercospora beticola*, *Phytophtora cinnamomi*, and *Sclerotinia sclerotiorum*[13] according to the authors, 1,8-cineole (Figure 1.4) showed the highest inhibitory effect. Another example is an unidentified *Diaporthe* (=*Phomopsis*) endophyte from *Odontoglossum* sp. producing abundant 3-methylbutanol (Figure 1.5) and sabinene (Figure 1.6) along with other 11 VOCs, which effectively inhibited the growth of *Aspergillus fumigatus*, *Fusarium solani*, *Geotrichum candidum*, *Pythium ultimum*, *P. cinnamomi*, *Phytophthora palmivora*, *Rhizoctonia solani*, and *S. sclerotiorum* by over 40% compared to their controls.[14]

Gas chromatography-mass spectrometry (GC-MS) and solid-phase microextraction (SPME) have facilitated the detection and discovery of VOCs.[15] The constantly increasing wealth of information in databases has helped the annotation and further evaluation of VOCs as long-distance mediators among microorganisms.[16,17] To ensure the accurate detection of VOCs during HS-SPME-GC-MS analysis, it is crucial to consider the configuration and equipment setup. A careful selection of columns and SPME fibers is necessary for detecting a wider range of compound families.[18] Polydimethylsiloxane (PDMS) is the commonly used nonpolar coating for SPME, thanks to its thermal stability and nonpolar affinity.[19] In recent studies on VOCs produced by fungi, the PDMS fiber has been the preferred option for their detection.[20−22]

There is a scarcity of accessible databases for ultrahigh-performance liquid chromatography coupled to mass spectrometry (UHPLC-MS/MS) analysis, which makes identifying compounds challenging. LC-MS/MS metabolomics is subject to variation depending on the equipment and detection technology used, which makes the standardization of data difficult.[23] Nevertheless, LC-MS/MS can provide information on most molecules present in an extract, and while public databases for metabolomic studies are expanding, most of them are currently focused on human metabolites, with databases for metabolites from bacteria and plants being developed at a later stage.[24] This highlights the importance of the microbeMASST initiative, soon to be published by the Dorrestein group, where thousands of annotated and raw MS/MS experiments from microorganisms will be available to the scientific community (https://masst.ucsd.edu/microbemasst/).

The American leaf spot of coffee (*Mycena citricolor*) is currently restricted to Central and South America, causing severe damage to coffee plants, including fruit and leaf drop contributing to economic losses.[25] Despite the lack of information about all of the factors favoring the spread of this pathogen, intense and prolonged rainy seasons have been identified as one of the main ones. For instance, in Costa Rica, between 2010 and 2011, the country estimated a loss of up to 60 million USD.[26−28] Globally, pathogens are responsible for around 40 billion USD in crop losses.[29,30] The use of agrochemicals continues to be the most common strategy for pathogen control despite the well-known negative impacts of their use.[31] Endophytic fungi are emerging as suitable alternatives to hazardous agrochemicals.[32] Moreover, endophytic fungi have shown the ability to promote growth and provide other beneficial effects to their hosts.[33] For example, in a recent study, several species of endophytes from wild Rubiaceae plants from Costa Rica were effective against *M. citricolor* in vitro and in planta, reducing disease incidence and severity and promoting plant growth.[34] However, that study hinted only at potential mechanisms of fungicidal or fungistatic effects. Understanding those mechanisms against pathogens, with specific interest in the release of metabolites possessing protective capabilities for essential crops, could lead to the development of effective alternatives for disease control.[35]

Among the isolates studied by Escudero-Leyva et al.,[34] *Daldinia eschscholtzii* GU11N, obtained from the plant *Randia grandifolia* (Rubiaceae), had an antagonistic effect over *M. citricolor* in an in vitro dual culture experiment. In that study, antibiosis was hypothesized as the mechanism of antagonism. *Daldinia* (Hypoxylaceae, Xylariales, Sordariomycetes, Ascomycota) species are producers of VOCs with fungicidal/fungistatic effects against different pathogens.[36,37] Recent examples include inhibitory effects against pathogenic microorganisms such as *Aspergillus niger*,[38] *Colletotrichum acutatum*,[39] *P. palmivora*,[40] and even nematodes.[41] Benzeneethanol (Figure 1.7), 1-methyl-1,4-cyclohexadiene (Figure 1.8), 3-methoxy-2-naphtol (Figure 1.9), and 3,5-dimethyl-4-heptanone (Figure 1.10) have been identified as common VOCs through the HS-SPME-GC-MS analysis.

To investigate the potential role of VOCs in the antagonistic effect of the endophytic isolate *D. eschscholtzii* GU11N against the coffee pathogen *M. citricolor*, a comprehensive analysis of the volatile chemical profile of *D. eschscholtzii* GU11N was conducted in the presence and absence of the pathogen using HS and HS-SPME-GC-MS analysis. Additionally, we examined the extracted metabolites from the confrontation zone and extracts from both fungi grown independently by using ultrahigh-performance liquid chromatography coupled to high-resolution mass spectrometry (UHPLC-HRMS/MS) to identify potential metabolites associated with the inhibitory

https://doi.org/10.1021/acsomega.3c03865
ACS Omega 2023, 8, 31373−31388

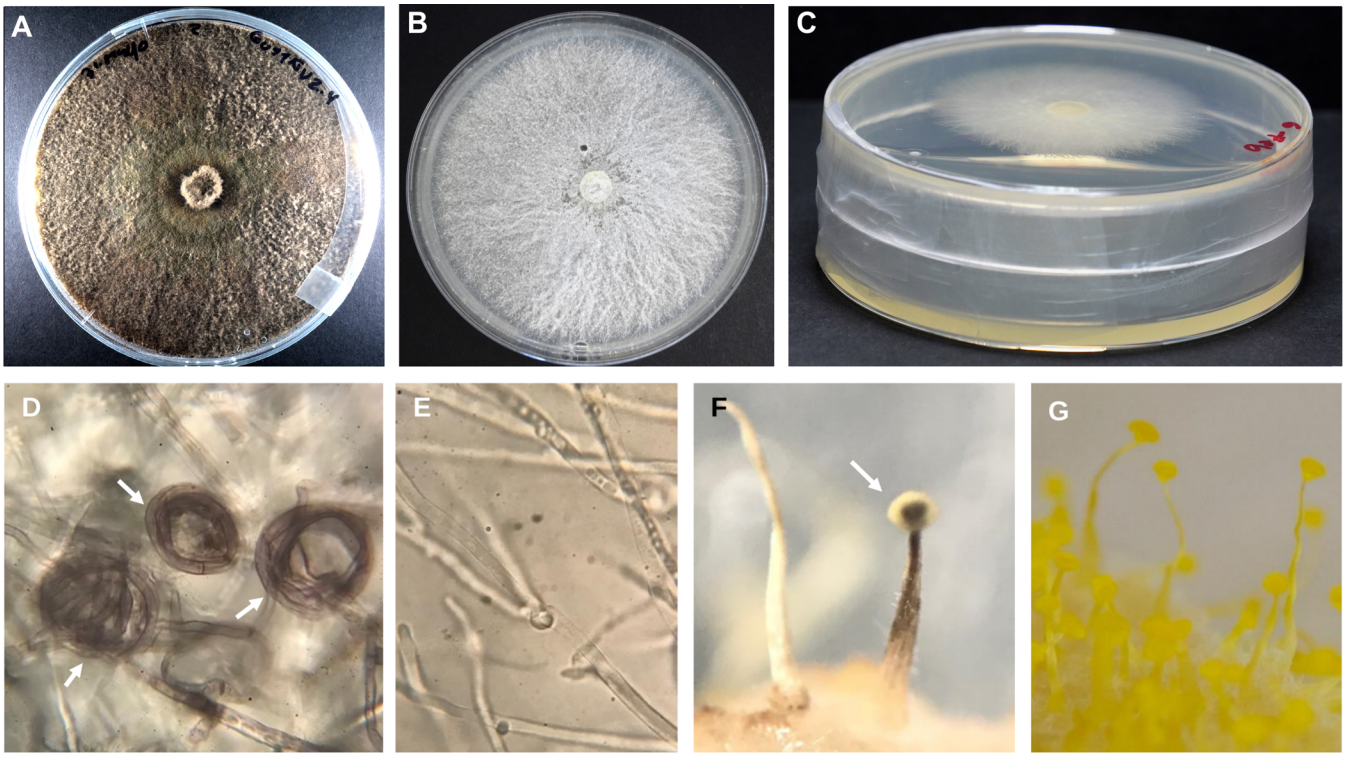

Figure 2. (A) Culture of *D. eschscholtzii* GU11N. (B) Culture of *M. citricolor*. (C) Contactless culture experiment. *M. citricolor* was placed on the top plate. (D) Hyphal damage in *M. citricolor* in the contactless culture experiment; coiled and burned-like hyphae are shown. (E) Normal hyphal growth in *M. citricolor* alone. (F) *M. citricolor* pseudopileus damage in the contactless culture experiment. The abundance of pseudopilei was reduced, and the structures presented a burned-like effect. (G) *M. citricolor* normal pseudopilei; abundant and bright yellow-colored pseudopilei growing without the presence of *D. eschscholtzii* GU11N.

effects. Our primary objectives were (i) to assess the impact of fungal volatile components from *D. eschscholtzii* GU11N on the pathogen within a closed system, (ii) to evaluate the volatile profile of *D. eschscholtzii* GU11N in the presence or absence of the pathogen, and (iii) to determine whether the inhibitory effect could also be attributed to nonvolatile components.

RESULTS AND DISCUSSION

Contactless Experiment. Previous studies have documented the bioactive effects of fungi producing VOCs in enclosed systems, specifically investigating inhibition or growth reduction of specific pathogens (mycofumigation) and even with seeds and fruits placed in proximity to the fungal isolates.[10,38,42] Our contactless experiment revealed that *D. eschscholtzii* GU11N exhibited a fungicidal rather than fungistatic effect against *M. citricolor*. Although there was no significant difference in the mycelial growth of *M. citricolor* between samples in the presence and absence of *D. eschscholtzii* (Figure S1), damaged pseudopilei or mycelial fragments failed to grow even with ample time and suitable media, indicating the potential fungicidal effect of *D. eschscholtzii*. Macroscopic damage occurred in all replicates of *M. citricolor* in the contactless experiment with *D. eschscholtzii* (Figure 2A−C). After 7 days, the damage observed in a 40× light microscope was seen as coiled and burned-like hyphae (Figure 2D). Segments displaying visible signs of damage were excised from hyphae and pseudopilei and transferred to a Petri dish containing fresh PDA media. After a five-day incubation period, no growth was observed in any of the fragments collected from the contactless experiment. Additionally, a reduction in the mycelial density and "burned" pseudopilei was observed (Figure 2F). However, *Mycena* radial growth, both in the presence and absence of *D. eschscholtzii*, exhibited no significant difference (Figure S1). Since *M. citricolor* pseudopilei infect coffee leaves, an assay involving the propagation and evaluation of *D. eschscholtzii* colonizing the leaf tissues and then evaluating its protective effect would be a promising future study. The results of such a study could provide answers to questions related to the mechanisms and responses in the plant−endophyte−pathogen system, where the effect seen under in vitro conditions could be different from that in an exposed environment, where numerous factors happen at the same time (e.g., temperature, humidity, UV radiation). In addition, testing and applying extracts (e.g., as an aerosol or spray application) of *D. eschscholtzii* GU11N's bioactive compounds may provide more evidence on mechanisms or strategies for their delivery.[43]

GC-MS Analysis and Metabolite Identifications. Fungal VOCs are a complex mixture of compounds,[44] making their identification challenging. To address this, the implementation of HS techniques associated with GC-MS is crucial for a more comprehensive analysis. Based on the observations from the contactless experiment, it is evident that an effect occurred in the volatile compartment shared by the coffee pathogen and the fungal endophyte. Direct sampling of this contactless experiment is difficult, which is why we opted to sample from a coculture experiment, segmenting the area near the confrontation zone where the two cultures almost meet. The experimental design involved the use of 10 replicates to improve the reproducibility in the biological samples. From each Petri dish, five agar plugs were sampled and placed in a vial for GC-MS analysis. Similarly, 10 replicates from *D. eschscholtzii* GU11N

https://doi.org/10.1021/acsomega.3c03865
ACS Omega 2023, 8, 31373−31388

and 10 replicates from *M. citricolor* were sampled and used as controls.

Data processing of the VOC profiling was performed in two separate ways: uploading the GC-MS raw data to the Data Analysis workflow on the GNPS platform[45] and deconvoluting using MZmine 2 (*v* 2.53).[46] The latter resulted in a more manageable feature table and therefore was used for further analyses (a feature corresponds to a chromatographic peak with a specific mass-to-charge ratio (m/z), retention time (RT), and intensity/area). It contained a total of 40 features derived from the samples of *D. eschscholtzii* GU11N agar plugs (D group) and those from the coculture experiment. The samples from *M. citricolor* plugs (M group) produced no volatiles. HS and HS-SPME experiments were processed independently, but the annotation results were combined in a final consensus annotations list (Table 1). As expected, HS-GC-MS identified a smaller number of VOCs than HS-SPME-GC-MS. Only 12 features were shared between both analysis techniques. A total of 26 features were identified exclusively using SPME. Table 1 presents the retention times, compound names, and chemical classes as well as the experimental and literature Kovats indexes (KIs) for the identified VOCs. The columns containing the up and down arrows were built upon the analysis of variance (ANOVA) analysis, indicating the relative concentration of each feature in the correspondent sampling experiment (HS or SPME). The chemical class of the features was determined using NPClassifier[47] directly from the structural annotation. The KIs shown in Table 1 are usually used for refining the annotations in untargeted metabolomics.[48] Caution is necessary when comparing the indexes due to evolving GC column materials. Nevertheless, KIs remain a powerful piece of information.[49]

The identity of the compounds was then validated with the comparison of the experimental KI and those reported in databases along with the hit rates (HRs) and similar score values, like the cosine provided by the GNPS platform. With all these factors, the identification level (from I to IV)[50] was suggested, being level I when the annotated feature was compared to a standard. Nonetheless, after an exhaustive search in databases, two features remained unknown (**33** and **35**).

It is important to address the differences obtained with the two sampling techniques, HS and HS-SPME (Table 1). The head volume in the first technique usually contains large quantities of carbon dioxide and water, with the latter coming from the sample. The presence of both components makes detection of other analytes difficult at the beginning of the chromatographic run. However, the absence of additional contaminants, such as fiber components, enables the detection of analytes in moderate quantities after the first 2 min.[15] On the other hand, the volatile profile obtained with HS-SPME depends on the polarity of the selected fiber coating. Typically, the PDMS-coated fiber is preferred for detection of low-molecular-weight compounds due to the thermal stability and nonpolar affinity.[19] Other available coatings such as carbowax or polyacrylate may allow the detection of more polar and therefore less volatile components.[15] Here, we selected a 100 μm PDMS-coated fiber when comparing its performance to that of a carbowax fiber. The chemical nature and molecular weights of the determined compounds led to the conclusion that the selection of the fiber was appropriate. Finally, although it is not surprising that with HS-SPME-GC-MS, more VOCs were detected, it is fair to say that the identified features in HS-GC-MS represent more accurately the chemical space involved in the contactless experiment.

Neither set of results (HS or HS-SPME) allowed for robust statistical analysis. Attempts to use internal standards for the quantification of VOCs and comparison of runs were unsuccessful. Consequently, we performed ANOVA using the features that were shared in both techniques for principal component analysis (PCA) and PLS-DA.

To determine if there are statistical differences between VOC levels between the D group and the coculture, an ANOVA was conducted for each sampling method (see Figure S2). In most of the detected features from both sampling methods, a consistent tendency of either increase or decrease was observed when comparing groups, as seen in features **5**, **7**, or **16.** However, features **22** and **27** exhibited contrasting prevalences depending on the specific sampling tool used. Among the listed features, namely, **19**, **21**, **25**, **26**, **37**, and **40**, these were more concentrated in the coculture when sampling with SPME (Table 1). Furthermore, VOC profiles for HS and HS-SPME revealed variations in their concentrations as stated before. The sampling method influences the levels and composition of identified VOCs as stated before. HS sampling provides a broader perspective on the volatile chemical profile, while HS-SPME analysis offers a more targeted and sensitive approach to specific compounds.

The ANOVA revealed significant differences in the VOC compositions between the D group and the coculture group. The D group showed higher levels of 4,4-dimethyl-1,3-cyclopentanedione (**7**), 1,2-dimethyl-4-oxocyclohex-2-enecarbaldehyde (**16**), α-selinene (**28**), and pogostole (**36**), all of which were statistically significant ($p < 0.05$). In contrast, the coculture group showed significantly higher levels of 9-epi-β-caryophyllene (**25**) and 1,8-dimethoxynaphthalene (**37**). These findings suggest that the interaction between *D. eschscholtzii* GU11N and the pathogen in the coculture experiment influences the production of specific VOCs, leading to distinct chemical profiles compared to *D. eschscholtzii* GU11N alone.

When using the complete set of features (40), the best 10 features detected as VIPs in the PLS-DA differ from the loadings obtained from the PCA. However, when performing the ANOVA of the data, it aligned best with the results from the PCA (Supporting Information: PCA and PLS-DA results for HS-SPME data). Therefore, variables or features identified as significant by ANOVA also contribute significantly to the separation between the groups in the PCA plot. The discrepancy between VIPs, PCA, and ANOVA can be a result of variables that may be highly correlated with each other, the presence of outliers, or the sample size. The set of biological replicates used in the experiment was 10 per group, whereas the number of variables was 40. Therefore, in this kind of experiment, where the number of identified VOCs is typically a small number, the number of samples should be increased to obtain data that can be best analyzed using multivariate approaches.[51] One way to circumvent this with the results at hand is to judiciously reduce the number of variables. Along this line, if the set of SPME variables to use ignores those variables that were absent in the HS experiments, the number of variables is reduced to 12. By performing this reduction on data, the PCA considered compound **37** as the only loading associated with the coculture samples (Figure 3A), PLS-DA scores acquired 59% cumulative variance, maintaining the D and coculture clusters, and the VIPs included 9-epi-β-caryophyllene (**25**) and 1,8-dimethoxynaphthalene (**37**), whose concentrations were higher in the coculture (Figure 3B). The last leads us to test the effect of these

https://doi.org/10.1021/acsomega.3c03865
ACS Omega 2023, 8, 31373−31388

Table 1. Volatile Organic Compound's Consensus List Identity[a]

features	RT (min)	compound name	chemical class[b]	D HS	coculture HS	D SPME	coculture SPME	KI experimental	KI Adams	KI NIST	annotation level[c]	% HR
1	5.46	2-methyl-1,3-pentanediol	fatty alcohols	nd	nd	↑	↓	930	-	959	III	77
2	5.55	2-ethyl-1-hexanol*	fatty alcohols	↑	↓	↑	↓	935	-	1030	III	83
3	6.30	1-octen-3-ol	fatty alcohols	nd	nd	=	=	977	-	981	III	83
4	6.49	1-nonen-3-ol*	fatty alcohols	↑	↓	nd	nd	987	-	1081	III	84
5	6.59	3-octanone*	oxygenated hydrocarbons	↑	↓	↑	↓	992		989	II	91
6	6.76	3-octanol*	fatty alcohols	nd	nd	↑	↓	1002	-	993	III	88
7	7.14	4,4-dimethyl-1,3-cyclopentanedione[d]	aliphatic ketone[e]	↑	↓	↑	↓	1024	-	1077	III	83
8	7.80	2,4-dimethyl-1-heptanol	fatty alcohols	nd	nd	↑	↓	1062	-	1030	III	77
9	8.91	benzeneethanol*	phenylethanoids	nd	nd	↑	↓	1129	-	1120	II	96
10	9.68	methyl 3-hydroxy-2,4,4-trimethylpentanoate	wax monoesters	nd	nd	↑	↓	1178	-	1097	IV	74
11	10.04	2-((3,3-dimethyloxiran-2-yl)methyl)-3-methylfuran	acyclic monoterpenoids	nd	nd	↑	↓	1202	-	1177	III	75
12	10.17	1-(1-cyclohexen-1-yl)-1-propanone	aliphatic ketone[e]	nd	nd	↑	↓	1210	-	1126	IV	70
13	10.25	heptyl 2,2-dimethylpropanoate	wax monoesters	nd	nd	↑	↓	1216	-	1263	IV	70
14	10.63	2,2,4,6-tetramethyl-3,5-heptanedione	fatty acids	nd	nd	↑	↓	1242		1174	III	79
15	10.83	1-acetyl-2-ethylidenecyclohexanol	aliphatic alcohol[e]	nd	nd	↑	↓	1256	-	1350	IV	70
16	11.05	1,2-dimethyl-4-oxocyclohex-2-enecarbaldehyde	aliphatic aldehyde[e]	↑	↓	↑	↓	1271	-	1285	IV	70
17	11.84	dihydro-5-pentyl-2(3*H*)-furanone	lactone	nd	nd	↑	↓	1327	-	1324	III	77
18	12.30	*α*-cubebene*	cubebane sesquiterpenoids	nd	nd	↓	↑	1361	1345	1351	II	92
19	12.35	2,2-dimethyl-1-(2-hydroxy-1-methylethyl) 2-methylpropionate	fatty acid ester[e]	nd	nd	↓	↑	1366	-	1347	IV	73
20	12.62	2-methylene-4,8,8-trimethyl-4-vinyl-bicyclo[5.2.0]nonane	caryophyllane sesquiterpenoids	nd	nd	↓	↑	1385		1407	III	84
21	12.68	*α*-copaene	copaane sesquiterpenoids	nd	nd	↓	↑	1390	1374	1375	III	87
22	12.88	*β*-elemene	elemane sesquiterpenoids	↓	↑	↑	↓	1404	1434	1390	II	92
23	13.31	*β*-caryophyllene*	caryophyllane sesquiterpenoids	nd	nd	=	=	1439	1417	1408	II	94
24	13.48	*α*-guaiene*	guaiane sesquiterpenoids	↑	↓	↑	↓	1452	1437	1439	II	92
25	13.55	9-epi-*β* -caryophyllene*	caryphyllane sesquiterpenoids	↓	↑	↓	↑	1458	1464	1461	II	96
26	14.00	5-hydroxy-2-methylchroman-4-one	chromones	nd	nd	↓	↑	1495	-	1608	III	76
27	14.16	*β*-selinene	eudesmane sesquiterpenoids	↓	↑	↑	↓	1507	1489	1492	II	90
28	14.26	*α*-selinene	eudesmane sesquiterpenoids	↑	↓	↑	↓	1516	1498	1517	II	90
29	14.36	*δ*-guaiene	guaiane sesquiterpenoids	↓	↑	↑	↓	1524	-	1526	II	90
30	14.40	hexamethylcyclohexane-1,3,5-trione	simple cyclic polyketides	nd	nd	↑	↓	1527	-	1637	IV	72
31	14.65	*β*-vetivenene	eremophilane sesquiterpenoids	nd	nd	↑	↓	1548	-	1540	IV	72
32	15.13	3,4-dimethoxyphenylacetone*	aromatic ketone[e]	nd	nd	↑	↓	1587	-	1507	IV	74
33	15.21	ni	aromatic compound[e]	nd	nd	↑	↓	1596			IV	
34	15.38	*β*-atlantol*	bisabolane sesquiterpenoids	nd	nd	↑	↓	1610	-	1548	IV	87*
35	15.45	ni	aromatic compound[e]	nd	nd	↑	↓	1616	-	-	IV	
36	16.15	pogostole	guaiane sesquiterpenoids	↑	↓	↑	↓	1679	-	1655	II	96

https://doi.org/10.1021/acsomega.3c03865
ACS Omega 2023, 8, 31373−31388

Table 1. continued

features	RT (min)	compound name	chemical class[b]	D HS	coculture HS	D SPME	coculture SPME	KI experimental	KI Adams	KI NIST	annotation level[c]	% HR
37	16.20	1,8-dimethoxynaphthalene*	naphthalenes and derivatives	↓	↑	↓	↑	1685	-	1641	I	92
38	17.00	3,5,6,7,8,8a-hexahydro-4,8a-dimethyl-6-(1-methylethenyl)-2(1H) naphthalenone	eudesmane sesquiterpenoids	nd	nd	↑	↓	1760	-	1781	III	78
39	19.23	(*E*,*E*)-3,7,11,15-tetramethyl-1,6,10,14-hexadecatetraen-3-ol*	acyclic monoterpenoids	nd	nd	↑	↓	1940	-	2020	III	79
40	20.04	(*E*)-15,16-dinorlabda-8(17)-12-dien-14-al	norlabdane diterpenoids	nd	nd	↓	↑	1999	-	1967	III	88

[a]The putative identification for the compounds detected using HS and HS-SPME techniques is shown. Symbology: nd (not detected); ni (not identified); ↑ and ↓ (an increment and reduction); = (no difference of expression). D: Daldinia eschscholtzii GU11N; KI: Kovats index; HR: hit rate; RT: retention time. [b]NPClassifier ontology.[47] [c]Based on Schymanski et al.[50] All features were annotated using NIST 2020 and Wiley 2014 and, if needed, deconvolution with AMDIS before contrasting with the libraries. Consensus RT and area integration were made after deconvolution using MZmine 2.53. Annotation levels are as follows: level I: standard confirmation; level II: all features having a hit rate of ≥90% and $\Delta RI \leq 10$ IU; level III: all features having a hit rate of >75% and a $100 \leq \Delta RI > 10$ iu; and level IV, all of the rest. KI 1176. Pherobase (www.pherobase.com). [d]*Features with >0.8 cosine on a GNPS annotation exercise. [e]Manual annotations for the chemical class.

compounds against the *M. citricolor* reproductive structures, as explained further.

The composition of the chemical classes based on NPClassifier, relative to the number of features, is displayed in Table S1 and Figure S4. The two most represented classes for the D and coculture groups in HS were fatty alcohols (51.2%) and aliphatic ketones (33.9%) and caryophyllene-like sesquiterpenes (46.8%) and fatty alcohols (30.7%), respectively (Figure S5A). In the HS-SPME experiment, aliphatic ketones (16.9%), chromones (16.6%), aliphatic aldehydes (14%), and guaiane sesquiterpenes (11.9%) represented the D group, while the coculture was characterized by chromones (43.8%), naphthalenes and derivatives (31.8%), and caryophyllene-like sesquiterpenes (21.1%, Figure S4B,C).

According to the literature, VOCs previously detected for *D. eschscholtzii* GU11N include alcohols, chromones, and other aromatic compounds, dienes, ketones, aldehydes, and sesquiterpenes.[38,39,52] Among the volatile compounds that have shown statistical significance, we found α-cubebene (**18**), α-bisabolene, and guaizulene. These terpenes can cause damage to hyphal membranes and suppress conidial formation in *A. niger*.[53] Yet, the production and role of sesquiterpenes in fungi is highly variable and might include benefits for plant growth promotion (e.g., β-caryophyllene (**23**))[18] or detrimental effects like the correlation of the incidence of entomopathogenic pests and the emission of α-copaene (**21**).[54,55] The latter has been found to play a role in guiding females toward males and influencing reproductive success.[56] Most of the level-two annotated compounds were identified as sesquiterpenes. Benzochromenes are frequently reported for endophytic fungi. The chromanone 5-hydroxy-2-methylchroman-4-one (**26**) was also found in the endophytic fungus *Cryptosporiopsis sp.* and presented cytotoxic activity against leukemia cells.[57] Other chromenones displayed phytotoxic activity by affecting the mitochondrial membrane of mono- and dicotyledonous plants.[58] The isolate MFLUCC I9-0493, identified as *Daldinia eschscholtzii*, demonstrated significant inhibition of *C. acutatum* in coculture, with elemicin identified as the responsible inhibitor. Similarly, *Daldinia* cf. *concentrica* displayed inhibitory effects against 17 pathogenic fungi, leading to inhibitory ranges spanning from 30 to 100%.[39] In that study, the presence of 4-heptanone and *trans*-2-hexenal was correlated to the observed inhibition. Testing the inhibitory effect using synthetic compounds of these substances demonstrated an enhancement in inhibition performance; however, herbicidal effects were also noted.[38] *Daldinia bambusicola* effectively inhibited the pathogens *Colletotrichum lagenarium* and *P. palmivora*, while *A. alternata*, *B. cinerea*, and *Geotrichum* sp. were less affected (~60% of inhibition).[40] The major components detected in that study were benzeneethanol and 2*H*-1-benzopyran-2-*O*-methoxy-4,7-dihydroxy; however, none of these compounds was individually or collectively tested. In our findings, benzeneethanol was detected in *Daldinia eschscholtzii* GU11N. However, it did not show a difference in its concentration level when compared with the coculture experiment. On the contrary, its expression tended to decrease when *D. eschscholtzii* was exposed to *M. citricolor*. The implementation of sensitive techniques, such as HS-SPME, can enhance our understanding of ecological relations between microorganisms and the environment.[59] On the other hand, complementing these studies with preparative isolation and chemical characterization with tools like nuclear magnetic resonance (NMR) and liquid chromatography-mass spectrometry (LC-MS) is crucial for obtaining a comprehensive chemical

https://doi.org/10.1021/acsomega.3c03865
ACS Omega 2023, 8, 31373−31388

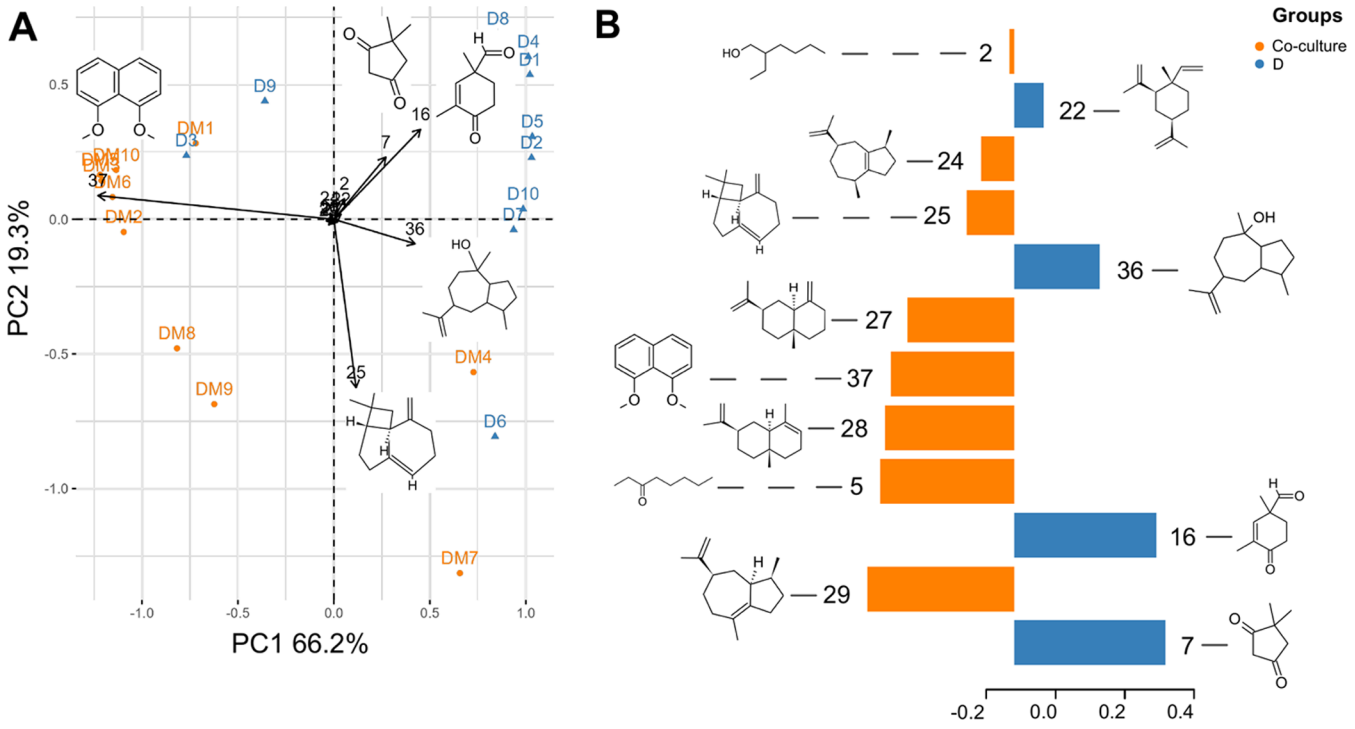

Figure 3. PCA and PLS-DA plots derived from the features present in the HS with HS-SPME data values. (A) PCA biplot with 85.5% cumulative variance. (B) PLS-DA VIPs for each group of the experiment (D and coculture).

annotation and biological testing to gain a better understanding of complex metabolic processes and ecological dynamics within communities.[60,61]

In Vitro Activity Test of Compounds against *M. citricolor* pseudopilei. Compound 1,8-dimethoxynaphthalene (**37**, synthesized from commercial 1,8-dihydroxynaphthalene) and a mixture of terpenes (commercial standard item containing β-caryophyllene) were tested at different concentrations to evaluate the effect on *M. citricolor* pseudopilei (Figure 4A,B). The mixture of terpenes (20, 200, and 2000 μg) did not produce any effect over the pseudopilei. On the other hand, the pseudopilei enclosed in the Petri dishes along with the filter discs loaded with 500 and 1000 μg of the compound 1,8-dimethoxynaphthalene (**37**) experienced the "burned-like" effect after 24 h at room temperature, which was similar to the damage observed when the pathogen was confronted against *D. eschscholtzii* GU11N (Figure 4C). None of the negative controls (solvents) produced an effect on pseudopilei. This suggests that **37** produced in the coculture group is responsible for the fungicidal effect. Pseudopilei from the controls and lowest concentrations were able to grow in PDA media and hyphae, as seen after 12 h (Figure 4D). Moderate fungicidal and herbicidal activity has been reported for **37** from an endophytic "*Nodulisporium*" sp. (also a Xylariales) isolate against *Microbotryum violaceum* and *Zymoseptoria* (=*Septoria*) *tritici* in the agar diffusion assay and did not present bactericidal activity.[62] Low inhibitory activity was reported for compound **37** obtained from an endophytic *D. eschscholtzii* isolate from a mangrove in Thailand[63] against *Microsporum gypseum* and *Staphylococcus aureus*. In addition, **37** was also reported from another *D. eschscholtzii* from the same ecosystem, but no activity tests were done.[64] Results from herbicidal tests performed in mono- and dicotyledonous plants have also been reported as low, retarding seed germination.[58] Another biological effect promoted by 1,8-dimethoxynaphthalene (**37**) is the more intense inhibition of the inflammatory process evaluated in murine macrophages when compared to quercetin; in this case, **37** was acquired from endophytic *Hypoxylon investiens*.[65]

Attempts to isolate fair amounts of volatile content and obtain pure compounds were not pursued. Therefore, the actual effect of this type of components on *M. citricolor* pseudopilei was not established, and the effects of **18**, **20**, **21**, **25**, **34**, **36**, and **38** remain unknown. Nonetheless, some works report effective fungicidal effects using terpenes obtained from plants and fungi and some modified derivatives using the disc diffusion method,[36,66,67] as well as by adding the essential oils directly into the culture media where conidia from pathogenic fungi have been previously inoculated.[68]

Comparing the pseudopilei morphology under SEM, notable changes were observed on the surface of the apical portion when they were exposed to 1,8-dimethoxynaphthalene (**37**). Undamaged structures remained turgent, with a consistent tapered shape (Figure 4E,F), whereas for those exposed to synthesized compound **37**, the original shape was obliterated, and the close-up details provided by the SEM photographs (Figure 4G,H) suggest damage related to wall or cell membrane disruption, leading to the fungicidal effect and germination inhibition. This kind of disruption to the fungal membranes is known from the exposure to synthetic (*E*)-2-hexanal at concentrations of 160 and 320 μL/L in a contactless experiment by altering the membrane permeability of *Penicillium aurantiogriseum* (= *Penicillium cyclopium*) conidia, producing a loss of lipids and potassium ions.[69] Similarly, conidia from *A. flavus* experienced membrane alteration and breakdown when exposed to the synthetic hexanal (3.2 and 9 μL/L), directly affecting the mitochondria, augmenting reactive oxygen species production, altering DNA replication, and promoting autophagy.[70] To our knowledge, this is the first time that this kind of effect has been reported, particularly for *M. citricolor* in confrontation against 1,8-dimethoxynaphthalene. Further analysis could include

https://doi.org/10.1021/acsomega.3c03865
ACS Omega 2023, 8, 31373−31388

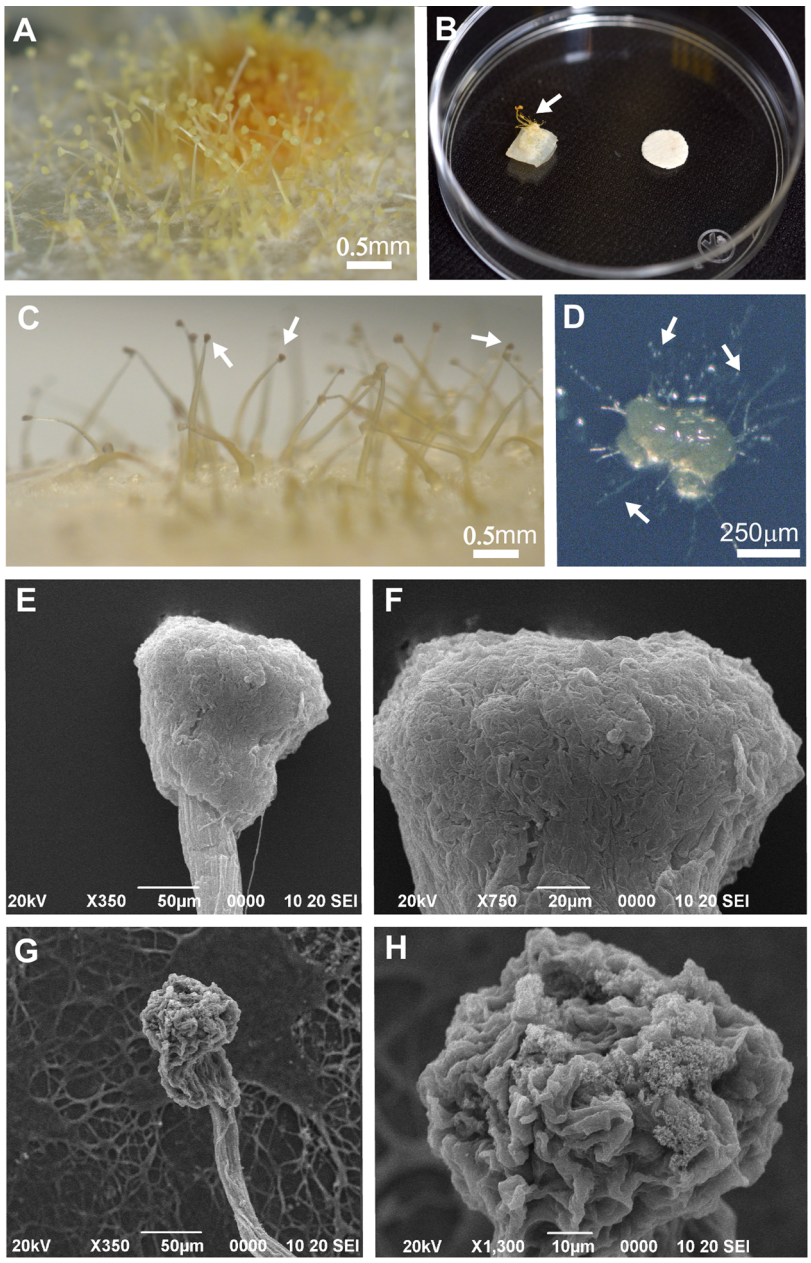

Figure 4. (A) Mature *M. citricolor* pseudopilei grown in PDA media. (B) Experiment with filter paper discs and *M. citricolor* pseudopelei (indicated by the arrow) in Petri dishes (6 cm diam.). (C) "Burning" effect (indicated by the arrow) produced in the pseudopilei in the presence of 1,8-dimethoxynaphthalene (500 and 1000 μg) after 24 h. (D) Pseudopilei from the control without damage and growing in PDA media after 12 h; arrows point to the developing hyphae. (E) SEM photograph from undamaged pseudopilei from the control group. (F) SEM details from the pseusopilei apical surface. (G) SEM image of the pseudopilei group exposed to 1,8-dimethoxynaphthalene (500 μg). (H) Detail of the damaged pseudopilei after exposure to 1,8-dimethoxynaphthalene.

transcriptomics to understand the changes at the metabolomic level and toxicity tests to evaluate the plant and human safety levels of exposure to this compound.

UHPLC-HMRMS/MS Profiling and Metabolite Annotation Overview. The UHPLC-HRMS/MS profiles obtained from the extracts of *Daldinia eschscholtzii* GU11N, *M. citricolor*, and the coculture were processed using MZmine 3.[71] This generated a table of 434 features (Table S2), which were then putatively annotated through the GNPS platform[72] and Sirius 5.[73] Results from both annotation strategies were consolidated and filtered to ensure a minimum of quality before any biological significance. This was done first with a pre-established workflow[74] followed by manual curation. The library search algorithm from GNPS was able to annotate only 5 out of 434 features. In contrast, Sirius provided a 21% annotation rate, while the module CANOPUS[75] was able to annotate 62.7% of the features with a chemical class. The quantitative .csv file was formatted using an in-house Python script to group the features according to the ion identity networking[76] results. The features were grouped based on their annotation network number (ANN), keeping only the highest intensity between the grouped features to perform statistical analysis. This resulted in only one ANN per metabolite, which reduced the number of adducts.

The PCA analysis based on this data showed that the samples from the coculture group formed a unique cluster in the upper left quadrant of the PC1 and PC2 plots, which accounted for

https://doi.org/10.1021/acsomega.3c03865
ACS Omega 2023, 8, 31373−31388

55.5% of the total variance (Figure S5). Loadings for features **255** (chemical class of amino acids/peptides) and **293** (chemical class of fatty acid derivatives) were observed in this cluster. Additionally, four coculture samples were grouped together with most of the M group in the right quadrants, with loadings for features **258** (MM 295.2456) and **280** (MM 297.2633) being the main contributors.

The distribution pattern of the *D. eschscholtzii* GU11N samples was evident in the PC2 and PC3 plots, which accounted for 33.1% of the total variance. Specifically, 6 out of the 10 *D. eschscholtzii* GU11N samples showed a correlation with feature **293**, along with four samples from the coculture group (refer to Figure S5A,B). The PLS-DA scores plot provided a clearer separation of samples from each group, allowing for distinct clustering of D, M, and coculture groups in the first two dimensions, explaining 45% of the total variance. From the top 15 VIP features from the first component of the PLS-DA analysis, features **298**, **252**, **247**, **295**, and **284** correlate strongly to the D group. Features **142**, **193**, **224**, **186**, **312** (*N*-acylethanolamine derivative), and **219** (tryptophan alkaloid) are more related to the M group, and features **293**, **62**, **311**, and **239** correlate to the coculture group (Table 2 and Figure S5C).

Table 2. Top 15 VIP Annotation Network Number (ANN) from the PLS-DA Analysis Based on the UHPLC-HRMS/MS Analysis

annotation network number (ANN) relevant in PCA and PLS-DA	group	NPClassifier superclass
62	coculture	purine alkaloids
142	M	-
186	M	pinane monoterpenoids
193	M	-
219	M	unsaturated fatty acids
224	M	-
239	coculture	-
247	D	open chain polyketides
252	D	fatty acyl carnitines
255	coculture	cyclic peptides
258	M	-
280	M	*N*-acyl amines
284	D	cholane steroids
293	D, coculture	fatty acyl carnitines
295	D	cholane steroids
298	D	phenylalanine-derived alkaloids
311	coculture	cholane steroids
312	M	-

Even though one of the current challenges in untargeted metabolomics is the confidence and availability of the spectra in databases, especially those derived from microorganisms such as fungi,[77] we were able to produce a putative feature annotation up to the chemical class level for the extracts obtained from the D, coculture, and M groups. Of the five annotations with statistical importance related to the coculture, only four were putatively annotated. In addition, an extract from an observed matter was released to the medium from *D. eschscholtzii* GU11N when confronted with *M. citricolor* and was submitted to LC-MS analysis. From the UHPLC-HRMS/MS data processing of this sample with MZmine 3, a total of 519 features were obtained and subsequently submitted to GNPS (4.8% annotation) and Sirius 5-CANOPUS (58.4%). As previously mentioned, most of the annotations must be revised and are, at this point, only proposals. The molecular networking derived from these data and supplied with the statistical values from the PLS-DA analysis represented in the size of each node displays some unique and shared annotations among the group samples (Figure 5). Among the clusters I, II, and III, the first one contains more diversity of chemical groups, being the most relevant for the D and the coculture, the node with a molecular weight of 191.6666 and categorized as an alkaloid. Among some of the shared nodes between D and M, many remain without a proposed annotation; nonetheless, nodes such as 332.2209 or 183.0934 are classified as amino acids, peptides, and alkaloids. Cluster II was better represented by the D and coculture groups; however, node 474.3799 was assigned to fatty acids and included a representation of the M group as well. Cluster III contains a node (520.3601) shared between the three sample groups cataloged as an alkaloid, but the node with more statistical significance was that labeled as 520.3618 and signaled as a fatty acid. Finally, cluster IV had an exclusive representation of the D and coculture groups, with fatty acids as the majority of the annotated nodes. Assuming that the coculture could contain compounds derived from both fungi growing in the coculture assay, and since the fungal cell membrane differs in its composition from plants and animals, compounds related to this structure may be pigments, e.g., 1,8-dihydroxynaphthalene, reported as common in *Aspergillus* spp.,[78] or lipids, from which ergosterol is a major component of the fungal cell membrane.[79] Undoubtedly, the coculture represents a rich metabolomic environment, containing fatty acids (45% of the annotations), terpenoids (14%), alkaloids (11.76%), polyketides (11%), amino acids and peptides (7%), carbohydrates (3.30%), and shikimates and phenylpropanoids (2.57%), leaving out 5.51% of the metabolites without annotation (Figure S7). To the best of our knowledge, no metabolite profiling has been done for *M. citricolor*, except for other *Mycena* or related saprophytic species (i.e., *Mycena hematopus* and *Mycena pruinosoviscida*). *M. hematopus* produced bactericidal pyrroloquinoline alkaloids[80] and pigments (e.g., hematopodins or mycenarubins).[81] *Mycena pruinosoviscida* (now *Roridomyces pruinosoviscida*) produced the fungicidal compounds phenylglycols and mycenadiols.[82]

Certainly, evaluation of the role of volatiles and nonvolatile compounds on fungi−fungi interactions poses several challenges from the methodological to the instrumentation capacities; however, this kind of research helps enlighten the metabolomic dynamics of fungal interactions.[83] This knowledge can be applied in the search for applications of fungal endophytes and their natural products to improve crop health, since several variables may shape the multispecies (e.g., plants−pathogens−endophytes) interactions;[84] for example, the chemistry of the plant itself that can affect an antagonistic effect seen in in vitro conditions.[85] In addition, with this knowledge, we can start to understand how multispecies interactions in natural conditions affect the overall phytobiome and, consequently, a plant's immunity and its relationship with other species and the ecosystem.

CONCLUSIONS

The endophytic isolate *Daldinia eschscholtzii* GU11N produced damage to the reproductive structures of the coffee pathogen *M. citricolor* in a contactless assay. Thirteen compounds were detected using HS and 39 by HS-SPME. With HS, the volatile

https://doi.org/10.1021/acsomega.3c03865
ACS Omega 2023, 8, 31373−31388

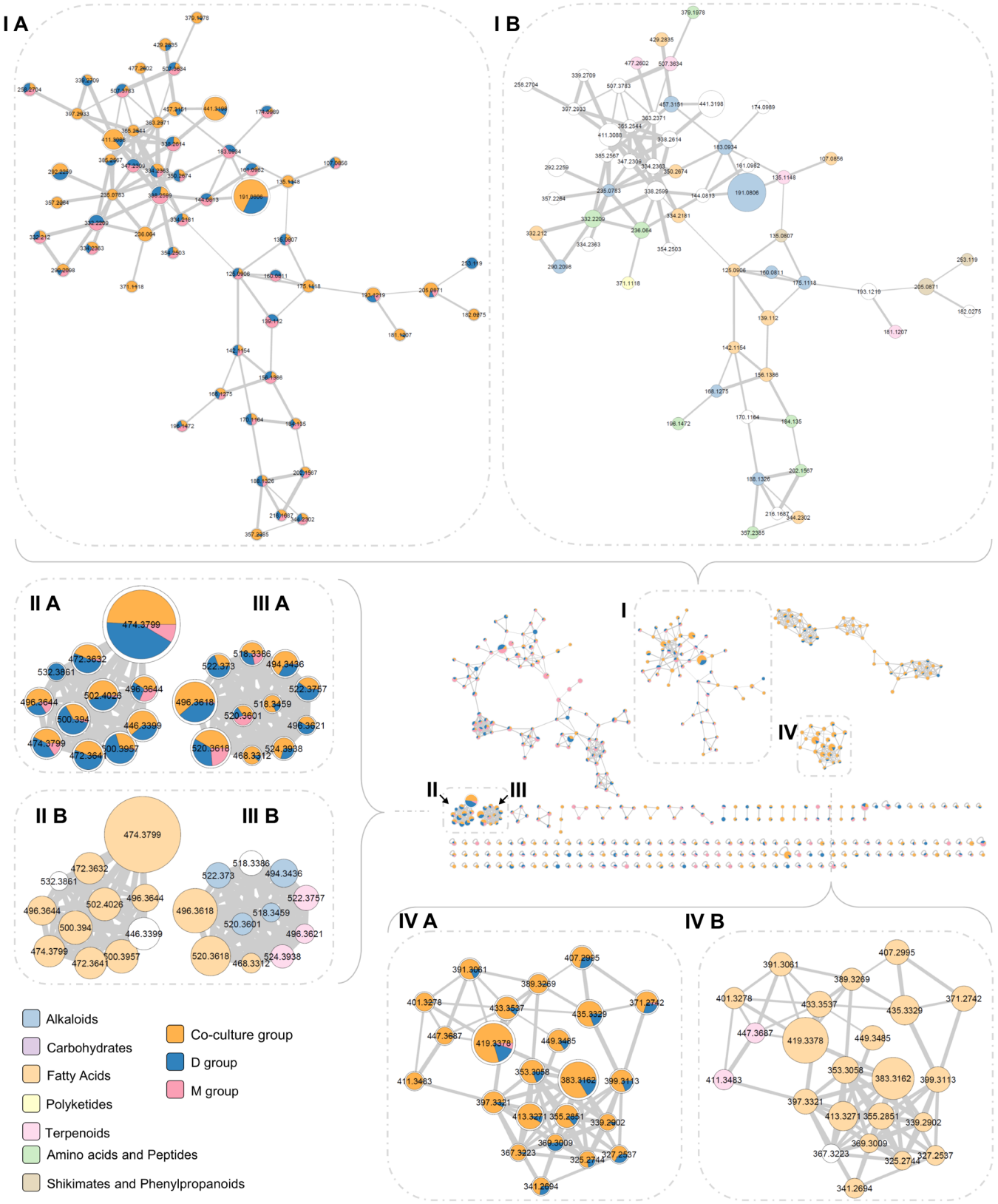

Figure 5. Molecular network derived from UHPLC data analysis. Node sizes represent the VIP value from the PLS-DA analysis. Node labels are molecular weights. Only the clusters with significant statistical values are displayed on a larger scale.

profile for *D. eschscholtzii* was represented by aliphatic ketones and fatty alcohols; sesquiterpenes were also detected. Using HS-SPME, the *D. eschscholtzii* profile was more diverse, detecting the classes found with HS in addition to chromones and polyketides as well as other sesquiterpenoid components. The composition of this profile revealed significant changes when the endophyte was exposed to *M. citricolor* in the coculture experiments. First, the HS profile showed increased detection

https://doi.org/10.1021/acsomega.3c03865
ACS Omega 2023, 8, 31373−31388

of caryophyllene sesquiterpenoids and naphthalenes and an evident suppression of aliphatic ketones. Similarly, the HS-SPME analysis added the detection of chromones. 1,8-Dimethoxynaphathalene (37) had a statistical correlation with the coculture experiment and produced the "burning" damage over the *M. citricolor* pseudopilei supported by microscopic observations (light and SEM microscopy); these images revealed severe damage to the reproductive structures possibly related to membrane disruption. A mixture of terpenes was tested without effects on the pathogen structures. UHPLC annotations demonstrate that the confrontation area was comprised mostly of fatty acids; followed by terpenoids, alkaloids, and polyketides in similar proportions, amino acids, and peptides; and finally, carbohydrates, shikimates, and phenylpropanoids in the smallest proportions. Understanding the changes derived from stress conditions, such as those produced by endophytic fungi emitting VOCs, could lead to the implementation of alternatives in agriculture for controlling important pests and to a better understanding of multispecies interactions in phytobiomes.

MATERIALS AND METHODS

Fungal Isolates. The endophytic fungus *Daldinia eschscholtzii* (isolate GU11N) was isolated from *R. grandifolia* leaves, while *M. citricolor* (isolate LAMYH1) was recovered from infected coffee plants from San Marcos de Tarrazu, Costa Rica. Both isolates were identified and used in a previous study by our research team.[34] Both fungi are preserved at −80 °C in cryovials with 20% glycerol and in sterile water at room temperature (~25 °C) in CIPRONA (University of Costa Rica) culture collection.

Contactless Experiment. The "sandwich" technique[38] was used for this experiment. Both fungi were grown in independent 90 mm Petri dishes with potato−dextrose agar (PDA, Difco Laboratories, Detroit, Michigan). The inoculum consisted of mycelial disks (~5 mm) placed 5 mm from the edge of the Petri dish. *Daldinia eschscholtzii* GU11N mycelial disks were placed on the bottom plate and those of *M. citricolor* on the top plate, facing *D. eschscholtzii* GU11N. Because the growth was faster in *D. eschscholtzii* GU11N, the pathogen was inoculated 2 days before starting the experiment. Radial growth (millimeters) of *M. citricolor* was measured every 24 h for 10 days. Ten replicates were done for the experiment. All plates were incubated at 25 °C with 12 h light/darkness cycles. Mycelia from *M. citricolor* treatments and control were observed under an Olympus BX40 light microscope and photographed with an attached 18 MP digital camera (Omax, China). Colony morphology was documented by using a Sony 6100 camera.

Coculture Assay. For this experiment, 90 mm Petri dishes with 20 mL of PDA were used to grow the *Daldinia eschscholtzii* GU11N (D group) and *M. citricolor* (M group) isolates independently and in a dual experiment with both fungi ("coculture") in the same plate. The coculture was done by placing mycelial disks 5 mm away from the plate's edge; in all treatments, the pathogen was placed 2 days before inoculating the *Daldinia* isolate. After 10 days, five mycelial discs from the edge of each independent culture and three from the confrontation line from the coculture experiment group were collected and placed inside 20 mL screw-top vials with poly(tetrafluoroethylene) (PTFE)/silicone septa caps (Thermo Scientific) for 24 h at 25 °C. Two vials with five PDA disks each were used as blanks along with three empty vials. Half of the mycelium from the independent cultures and the adjacent mycelium from the confrontation line were harvested using a sterile scalpel and stored in preweighted 20 mL vials and immediately lyophilized for 24 h (Labconco Freezone). After this, the vials were weighed to obtain mycelium yield.

HS and HS-SPME-GC-MS Data Acquisition. Vials with discs were pre-equilibrated for 15 min at 45 °C. A 100 μm PDMS SPME fiber (Thermo Scientific) was exposed to the sample headspace for 15 min at the same temperature with stirring in a TriPlus RSH autosampler (Thermo Scientific). Subsequently, the SPME fiber was thermally desorbed at 250 °C for 10 min in a GC-MS injector. Volatile compound measurements were conducted using a Gas Chromatograph Trace 1310 (Thermo Scientific) with a triple quadrupole mass detector TSQ 9000 system (Agilent Technologies), equipped with a TG-5MS capillary column (30 m length × 25 μm i.d. × 1 μm film thickness, Thermo Scientific). The injector of each sample was in split mode with a split ratio of 10, and the flow rate of the carrier gas (helium, 99.999% purity) was 1.2 mL/min. The temperature program was set as follows: initially, 60 °C for 3 min, increased to 200 °C at a rate of 10 °C/min, then increased to 290 °C at a rate of 15 °C/min, and finally maintained for 2 min. The gas chromatograph was set to ionization mode EI, 1 mL/min flow, mass range of 33−550 amu, transfer line at 280 °C, and ion source at 260 °C.

Data Processing with MZmine. The raw files from the HS-SPME experiment were converted from. RAW to an open. mzML format with MS Convert v3.0 Software.[86] Afterward, files were processed with MZmine v.2.5.3.[46] The noise level settled at 1E2 for only MS1. Parameters for the ADAP chromatogram builder were as follows: minimum group size in the number of scans, 5; group intensity threshold, 1E2; minimum highest intensity, 3E2; and m/z tolerance, 0.5. Settings for the ADAP chromatogram deconvolution were as follows: threshold, 8; estimator, "intensity window SN"; minimum feature height, 100; coefficient threshold, 5; peak duration range, 0.00−0.10; and retention time wavelet range, 0.01−0.11 min. Multivariate curve resolution was chosen as the spectral deconvolution option, and settings were adjusted as follows: deconvolution window width (min), 0.048; retention time tolerance (min), 0.08; and the minimum number of peaks, 4. For the deisotoped step, conditions were: m/z tolerance, 0.5; retention time tolerance, 0.08; maximum charge, 1; and representative isotope, "most intense". For the filtering process, the settings were as follows: m/z, 45.0000−250.0000; and retention time, 5.20−20.20 min. The final peak list was exported in .csv and .mgf formats for statistical analysis and spectral organization.

Spectral Organization through the GNPS platform. The online platform GNPS (Global Natural Products Social Network)[87] was used to upload the .mgf file and retrieve a molecular network. The settings were as follows: precursor ion mass tolerance, 0.02 Da; MS/MS fragment ion tolerance, 0.02 Da; and edges were filtered with cosine score >0.7 and >6 peaks. GNPS spectral libraries were used, and the conditions were to restrict a cosine score greater than 0.6 ad at least three matched peaks. Link for the job: https://gnps.ucsd.edu/ProteoSAFe/result.jsp?task=2ba96c07ebbb4bb29cca1659229be0f8&view=view_all_annotations_DB

Annotation through LabSolutions Postrun Analysis Software. The HS-SPME raw files were converted to CDF format using the Xcalibur v.4.2 (Thermo Scientific) Tool converter. The files were analyzed with LabSolutions Postrun Analysis software v.4 (Shimadzu Corporation) for compound annotation when the GNPS libraries did not offer a match for spectra. The peaks of each chromatogram were selected

https://doi.org/10.1021/acsomega.3c03865
ACS Omega 2023, 8, 31373−31388

following the retention time (RT) indicated by the MZmine feature list (Feature: a peak with an m/z value and area at a given retention time). Each selected feature on the spectrum table was compared against the Wiley 2014 and NIST 2020 databases requesting matches with similarity >80. This procedure was performed for each experiment group (D and M groups, and the coculture) and the blanks. The CDF files from the HS experiment were manually checked, and the RT for the features were corrected using the HS-SPME feature list; then, annotation for the compounds and area calculation was performed using the libraries and configuration described above.

Annotation through AMDIS Software. The NIST 20 mass spectral library v.1.0.8.8 loaded with MS Search v.2.4 and AMDIS 32 was used to corroborate the annotation features from the GNPS and LabSolutions platforms. The parameters used were as follows: the minimum match factor, 80; simple analysis; component width, 8; adjacent peak subtraction, 1; resolution, low; sensitivity, high; and shape requirements, medium.

Statistical Analysis for the GC-MS Data. The quantification table in .csv format obtained from the HS and HS-SPME experiments were normalized by the sum of each sample to perform ANOVA tests in R v.4.1.3.[88] Multivariate tests were done by applying Pareto scaling: principal component analysis (PCA) using the R FactoMineR v.2.4[89] and FactoExtra v.1.0.7[90] packages followed by partial least squares discriminant analysis (PLS-DA) with the mixOmics package v.6.6.2[91] in R v.3.5.1. A secondary analysis of PCA and PLS-DA for the HS-SPME data was done by using only the features detected as well in the HS experiment to fairly compare the detections for both tools.

In Vitro Activity Test of Synthetic Compounds against *M. citricolor* Pseudopilei. Filter paper discs (0.5 mm diameter) were saturated with 1, 10, and 100 μL of the terpene mixture (Supelco, CRM40937) by duplicate. The content of the third fraction (5.09 mg) corresponding to 1,8-dimethoxynaphthalene (Supporting Information: 1,8-dimethoxynaphthalene methylation) was resuspended in 509 μL of ether. Filter discs were saturated by triplicate with 10, 50, and 100 μL using a 100 μL syringe (Hamilton, Switzerland). The discs were air-dried and placed in Petri dishes (6 cm diameter) along with potato−dextrose−agar fragments containing previously grown *M. citricolor* pseudopilei (each fragment contained between 20−40 structures); the dishes were sealed using parafilm and left at room temperature (25 °C) and observed every 8 h with a dissecting microscope. After 24 h, three pseudopilei from each treatment were haphazardly removed and inoculated in Petri dishes with PDA to evaluate the germination and growth. Negative control for 1,8-dimethoxynaphthalene consisted of filter papers saturated with 500 μL of ether and those for the terpene mixture with the same amount of methanol (HPLC grade, J.T. Baker, Trinidad and Tobago); both control groups were performed in triplicate. Photographs in Figure 5A−D were taken using a DSLR camera (Nikon, D7100, Japan) with an 85 mm macro lens (Nikon, micro-Nikkor, Thailand), extension tubes (Vello), and wireless flashes (Nikon, SB-R200).

Scanning Electron Microscopy (SEM). The *M. citricolor* pseudopilei from the control and those with evident damage after exposure to 1,8-dimethoxynaphthalene were prepared and observed in the SEM (Jeol JSM-6390LV, Kyoto, Japan) at 20 kV; the magnification is specified in Figures 5E−H. For sample preparation, *M. citricolor* pseudopilei (around 25 per group) were immersed in 2.5% glutaraldehyde (0.1 M phosphate solution) at 4 °C for 24 h. Afterward, samples were washed with sterile water and dehydrated using sequential immersions of 20 min each in ethanol (from 30 to 95%). Finally, samples were vacuum freeze-dried, and a gold coating was applied (1 min, 1.8 mA, 2.5 kV).

UHPLC-HRMS Sample Preparation. The lyophilized samples were extracted following recommendations by Bertrand et al.[92] with two volumes of 10 mL of a dichloromethane/methanol/water (64:36:8) mix (HPLC grade, Merck), sonicated for 20 min in a water bath sonicator (Cole-Parmer) and filtered through cotton (previously washed with hexane, ethyl acetate, dichloromethane, and methanol all from Merck, LC-MS grade). Extractions were dried under a vacuum using a rotatory evaporator (Buchi, Switzerland). After being weighed, each sample was dissolved with methanol (HPLC quality, Sigma-Aldrich) to a 5 mg/mL concentration. To remove polar compounds and hyphae remnants, the methanol extracts were filtered through a solid-phase extraction cartridge (SPE) C_{18} (Chromabond, 100 mg, Macherey-Nagel, Germany), previously conditioned with 2 mL of methanol, 1:1 methanol/water, and 2 mL of water. Filters with a 0.2 μm nylon membrane (Millex, Merck, Ireland) were attached to the SPE columns, and the system was mounted in a vacuum chamber (SUPELCO Visiprep DL). Extracts were collected and dried under a vacuum using a Speed-Vac system (Savant Instruments). Samples were weighed and dissolved to 5 mg/mL in methanol (HPLC grade, Merck).

UHPLC-HRMS/MS Analysis. Analyses were performed with a Vanquish Duo UHPLC system (Thermo, Scientific, Germany) coupled to an Orbitrap Exploris 120 mass spectrometer (Thermo Scientific, Germany), employing a heated electrospray ionization source (H-ESI) with the following parameters: spray voltage: +3.2 kV; ion transfer tube temperature: 350.00 °C; vaporizer temperature: 400.00 °C; S-lens RF: 45 (arb units); sheath gas flow rate: 45.00 (arb units); and auxiliary gas flow rate: 15.00 (arb. units). The mass analyzer was calibrated using a mixture of caffeine, methionine−arginine−phenylalanine−alanine−acetate (MRFA), sodium dodecyl sulfate, sodium taurocholate, and Ultramark 1621 in an acetonitrile/methanol/water solution containing 1% formic acid by direct injection. Control of the instruments was done using Thermo Scientific Xcalibur 3.1 software v. 4.6.67.17. Full scans were acquired at a resolution of 60,000 fwhm (at m/z 200) and MS2 scans at 17,500 fwhm in the range of 100−1000 m/z, with 1 microscan, time (ms): 200 ms, an RF lens (%): 70; AGC target standard. The centroid data-dependent MS2 (dd-MS^2) scan acquisition events were performed in discovery mode, triggered by Apex detection with a trigger detection (%) of 75. The top 3 abundant precursors (charge states 1 and 2) within an isolation window of 2 m/z were considered for MS/MS analysis. Dynamic exclusion was set at 2 s. A mass tolerance of ±10 ppm was allowed, and the precursor intensity threshold was set at 150×10^3. For precursor fragmentation in the HCD mode, a normalized collision energy of 30% was used. The chromatographic separation was done on a Waters BEH C18 column (50 × 2.1 mm i.d., 1.7 μm, Waters, Milford, MA) using a linear gradient of 5−100% B over 13.50 min, followed by an isocratic step at 100% B until 15.50 min. The mobile phases were (A) water with 0.1% formic acid (Merck, grade HPLC-MS) and (B) acetonitrile with 0.1% formic acid (Merck, grade HPLC-MS). The flow rate was set to 500 μL/min, the injection volume was 2 μL, and the column was kept at 40 °C.

UHPLC-HMRMS/MS Data Processing. The raw data files were converted to. mzML format employing MS Convert software. The mzML files were processed with MZMine 3 software.[46] For mass detection at the MS1 level, the noise level

https://doi.org/10.1021/acsomega.3c03865
ACS Omega 2023, 8, 31373−31388

was set to 6.5E3. For MS2 detection, the noise level was set to 7.00. The ADAP chromatogram builder parameters were set as follows: minimum group size in the number of scans: 5; group intensity threshold: 7.0E5; minimum highest intensity: 1.4E6; and scan-to-scan accuracy (m/z): 0.0010 or 5.0 ppm. The local minimum feature resolver algorithm was used for chromatogram deconvolution with the following parameters: MS/MS scan pairing; check (default parameters); chromatographic threshold: 85%; minimum relative height: 0%; minimum absolute height: 7.0E5; minimum ratio of peak/edge: 4.90; peak duration range: 0.01−0.08; and min # of data points: 4. Isotopes were detected using the 13 °C isotope filter with an m/z tolerance of 0.0010 or 5.0 ppm, a retention time tolerance of 0.08 min (absolute), and the maximum charge set at 2. The representative isotope used was the most intense m/z. The files were aligned with the Join aligner algorithm (m/z tolerance: 0.0010 or 5 ppm; weight for m/z: 3; retention time tolerance: 0.08 min (absolute); weight for RT: 1), and the features present in the blanks were removed through the feature list blank subtraction algorithm (minimum number of detection in blanks: 3 and fold change increase: 300%). The resulting list was filtered by retention time: 2.70−7.30; features duration range: 0.02−1.0; and chromatographic fwhm: 0.01−1.0 with the feature list rows filter algorithm. The resulting filtered list was subjected to ion identity networking[76] starting with the metaCorrelate module (RT tolerance, 0.10 min; minimum height, 7.0E5; intensity correlation threshold 7.0E5, and the correlation grouping with the default parameters), followed by ion identity networking (m/z tolerance, 5.0 ppm; check: one feature; minimum height: 1.0E6; annotation library [maximum charge, 2; maximum molecules/cluster, 2; adducts ($[M + H]^+$, $[M + Na]^+$, $[M + K]^+$, $[M + NH4]^+$, $[M + 2H]^{2+}$), modifications ($[M - H_2O]$, $[M - 2H_2O]$, $[M - CO_2]$, [M + HFA], [M + ACN])]; annotation refinement (delete small networks without major ions, yes; delete networks without monomers, yes); add ion identities networks (m/z tolerance, 5 ppm; minimum height, 1.0E6; annotation refinement (minimum size, 1; delete small networks without major ions, yes; delete small networks: link threshold, 4; delete networks without monomers, yes); and check all ion identities by MS/MS (m/z tolerance (MS2), 10 ppm; min-height (in MS2), 1.0E3; check for multimers, yes; check neutral losses (MS1 → MS2), yes) modules. The resulting aligned peak list was exported as an .mgf file for further analysis.

Quantitative Data File Processing. The quantitative .csv file was formatted using an in-house python script to group the features according to the ion identity networking results. The features were grouped according to their annotation network number, keeping only the highest intensity between the grouped features.

Quantitative Data Statistical Analysis. The quantitative table in .csv format was normalized by the sum of each sample, and Pareto scaling was applied to perform principal component analysis (PCA) using the R FactoMineR v.2.4[89] and FactoExtra v.1.0.7[90] packages in R v.4.1.3.[88] Then, partial least squares discriminant analysis (PLS-DA) with the mixOmics package v.6.6.2[91] in R v.3.5.1 was performed.

Spectral Organization and Dereplication Process for Molecular Networking. The quantitative and spectral files obtained from MZmine were uploaded in the GNPS platform to generate feature-based molecular networking. The precursor ion mass tolerance was set to 0.02 Da with an MS/MS fragment ion tolerance of 0.02 Da. A network was created where edges were filtered to have a cosine score above 0.7 and more than six matched peaks. The spectra in the network were then searched against the GNPS' spectral libraries. All matches between network and library spectra were required to have a score above 0.6 and at least three matched peaks. Job link: https://gnps.ucsd.edu/ProteoSAFe/status.jsp?task=777a3645587a44aea28efc26d043a841

Metabolite Annotation with Sirius. The .mgf file exported from MZmine (using the SIRIUS export module) was processed with SIRIUS (v5.6.2).[73] The parameters were set as follows: possible ionizations: $[M + H]^+$, $[M + NH_4]^+$, $[M - H_2O + H]^+$, $[M + K]^+$, $[M + Na]^+$, and $[M - 2H_2O + H]^+$; instrument profile: Orbitrap; mass accuracy: 5 ppm for MS^1 and 7 ppm for MS2; database for molecular formulas and structures: BIO; and maximum m/z to compute: 1000. ZODIAC was used to improve molecular formula prediction using a threshold filter of 0.99.[93] Metabolite structure prediction was made with CSI: FingerID,[94] and significance was computed with COSMIC.[95] The chemical class prediction was made with CANOPUS[75] using the NPClassifier ontology.[47]

■ ASSOCIATED CONTENT

Supporting Information

The Supporting Information is available free of charge at https://pubs.acs.org/doi/10.1021/acsomega.3c03865.

> Synthesis of 1,8-dimethoxynaphthalene, including materials, purification, and characterization steps; mycelium growth measurements of *M. citricolor* under both unchallenged and challenged conditions; supplementary statistical analysis for GC-MS experiments and UHPLC-HRMS containing ANOVA (GC-MS only); complementary PCA biplot and PLS-DA with VIPs' figures and representations of the chemical ontology using the NPClassifier nomenclature; supplementary table showing the distribution of features using the chemical ontology for HS and HS-SPME; and supplementary table showing the process in MZmine for UHPLC-HRMS features (PDF)

■ AUTHOR INFORMATION

Corresponding Author

Giselle Tamayo-Castillo − *Centro de Investigaciones en Productos Naturales (CIPRONA), Universidad de Costa Rica, 11520-2060 San José, Costa Rica; Escuela de Química, Universidad de Costa Rica, 11520-2060 San José, Costa Rica;* orcid.org/0000-0002-4912-8895; Email: giselle.tamayo@ucr.ac.cr

Authors

Efraín Escudero-Leyva − *Centro de Investigaciones en Productos Naturales (CIPRONA), Universidad de Costa Rica, 11520-2060 San José, Costa Rica; Escuela de Biología, Universidad de Costa Rica, 11520-2060 San José, Costa Rica*

Luis Quirós-Guerrero − *Institute of Pharmaceutical Sciences of Western Switzerland, University of Geneva, 1205 Geneva, Switzerland; School of Pharmaceutical Sciences, University of Geneva, 1205 Geneva, Switzerland;* orcid.org/0000-0002-1630-8697

Víctor Vásquez-Chaves − *Centro de Investigaciones en Productos Naturales (CIPRONA), Universidad de Costa Rica, 11520-2060 San José, Costa Rica*

https://doi.org/10.1021/acsomega.3c03865
ACS Omega 2023, 8, 31373−31388

Reinaldo Pereira-Reyes − *Laboratorio Nacional de Nanotecnología (LANOTEC), Centro Nacional de Alta Tecnología, 10109 San Jose, Costa Rica*

Priscila Chaverri − *Centro de Investigaciones en Productos Naturales (CIPRONA), Universidad de Costa Rica, 11520-2060 San José, Costa Rica; Escuela de Biología, Universidad de Costa Rica, 11520-2060 San José, Costa Rica; Department of Natural Sciences, Bowie State University, Bowie, Maryland 20715, United States*

Complete contact information is available at: https://pubs.acs.org/10.1021/acsomega.3c03865

Notes

The authors declare no competing financial interest.

■ ACKNOWLEDGMENTS

The present manuscript was supported by U.S. National Science Foundation grant DEB-1638976 to P.C., and University of Costa Rica Vice-Rectory for Research projects B7176 and C1604. The isolate GU11N was collected under the SINAC-ACG permit ACG-PI-017-2017. The authors are thankful for the kind help from Lorena Hernández, David Morera, and Karolina Rivera, for their valuable assistantship in the laboratory during sample preparation. The authors acknowledge E.E.-L. for taking and providing the photographs included in this manuscript.

■ REFERENCES

(1) González-Teuber, M.; Palma-Onetto, V.; Aguilera-Sammaritano, J.; Mithöfer, A. Roles of leaf functional traits in fungal endophyte colonization: Potential implications for host−pathogen interactions. *J. Ecol.* **2021**, *109* (12), 3972−3987.

(2) Rodriguez, R. J.; Redman, R. S.; Henson, J. M. The role of fungal symbioses in the adaptation of plants to high stress environments. *Mitig. Adapt. Strateg. Global Change* **2004**, *9* (3), 261−272.

(3) Evans, H. C. The endophyte-enemy release hypothesis: implications for classical biological control and plant invasions. In *Proceedings of the XII International Symposium on Biological Control of Weeds, La Granded Motte, France, April 22−-27, 2007*; Julien, M.; Sforza, R.; Bon, M., Eds.; CABI: United Kingdom, 2008. DOI: 10.1079/9781845935061.0020.

(4) Quintana-Rodriguez, E.; Rivera-Macias, L. E.; Adame-Alvarez, R. M.; Torres, J. M.; Heil, M. Shared weapons in fungus-fungus and fungus-plant interactions? Volatile organic compounds of plant or fungal origin exert direct antifungal activity in vitro. *Fungal Ecol.* **2018**, *33*, 115−121.

(5) Cale, J. A.; Collignon, R. M.; Klutsch, J. G.; Kanekar, S. S.; Hussain, A.; Erbilgin, N. Fungal volatiles can act as carbon sources and semiochemicals to mediate interspecific interactions among bark beetle-associated fungal symbionts. *PLoS One* **2016**, *11* (9), No. e0162197.

(6) Rostás, M.; Cripps, M. G.; Silcock, P. Aboveground endophyte affects root volatile emission and host plant selection of a belowground insect. *Oecologia* **2015**, *177* (2), 487−497.

(7) Thomas, G.; Withall, D.; Birkett, M. Harnessing microbial volatiles to replace pesticides and fertilizers. *Microb. Biotechnol.* **2020**, *13* (5), 1366−1376.

(8) Hung, R.; Lee, S.; Bennett, J. W. Fungal volatile organic compounds and their role in ecosystems. *Appl. Microbiol. Biotechnol.* **2015**, *99* (8), 3395−3405.

(9) Kaddes, A.; Fauconnier, M. L.; Sassi, K.; Nasraoui, B.; Jijakli, M. H. Endophytic fungal volatile compounds as solution for sustainable agriculture. *Molecules* **2019**, *24* (6), 1065.

(10) Lee, S. O.; Kim, H. Y.; Choi, G. J.; Lee, H. B.; Jang, K. S.; Choi, Y. H.; Kim, J.-C. Mycofumigation with *Oxyporus latemarginatus* EF069 for control of postharvest apple decay and *Rhizoctonia* root rot on moth orchid. *J. Appl. Microbiol.* **2009**, *106* (4), 1213−1219.

(11) Kottb, M.; Gigolashvili, T.; Großkinsky, D. K.; Piechulla, B. *Trichoderma* volatiles effecting *Arabidopsis*: From inhibition to protection against phytopathogenic fungi. *Front. Microbiol.* **2015**, *6*, 995.

(12) Meshram, V.; Kapoor, N.; Saxena, S. *Muscodor kashayum* sp. nov. -a new volatile anti-microbial producing endophytic fungus. *Mycology* **2013**, *4* (4), 196−204.

(13) Tomsheck, A. R.; Strobel, G. A.; Booth, E.; Geary, B.; Spakowicz, D.; Knighton, B.; Floerchinger, C.; Sears, J.; Liarzi, O.; Ezra, D. *Hypoxylon* sp., an endophyte of *Persea indica*, producing 1,8-cineole and other bioactive volatiles with fuel potential. *Microb. Ecol.* **2010**, *60* (4), 903−914.

(14) Singh, S. K.; Strobel, G. A.; Knighton, B.; Geary, B.; Sears, J.; Ezra, D. An endophytic *Phomopsis* sp. possessing bioactivity and fuel potential with its volatile organic compounds. *Microb. Ecol.* **2011**, *61* (4), 729−739.

(15) Hübschmann, H.-J. *Handbook of GC-MS: Fundamentals and Applications*, 2nd ed.; McMaster, M., Ed.; Wiley & Sons, Inc.: Germany, 2015; pp 10−12.

(16) Sharifi, R.; Ryu, C. M. Sniffing bacterial volatile compounds for healthier plants. *Curr. Opin. Plant Biol.* **2018**, *44*, 88−97.

(17) Schalchli, H.; Hormazábal, E.; Becerra, J.; Briceño, G.; Hernández, V.; Rubilar, O.; Diez, M. C. Volatiles from white-rot fungi for controlling plant pathogenic fungi. *Chem. Ecol.* **2015**, *31* (8), 754−763.

(18) Guo, Y.; Werner, J.; Ghirardo, A.; Antritter, F.; Benz, J. P.; Schnitzler, J.-P.; Rosenkranz, M. Sniffing fungi − phenotyping of volatile chemical diversity in *Trichoderma* species. *New Phytol.* **2020**, *227* (1), 244−259.

(19) Shirey, R. E. SPME Commercial Devices and Fibre Coatings. In *Handbook of Solid Phase Microextraction*; Elsevier Inc., 2012; pp 99−133 DOI: 10.1016/B978-0-12-416017-0.00004-8.

(20) Xing, S.; Gao, Y.; Li, X.; Ren, H.; Gao, Y.; Yang, H.; Liu, Y.; He, S.; Huang, Q. Antifungal activity of volatile components from *Ceratocystis fimbriata* and its potential biocontrol mechanism on *Alternaria alternata* in postharvest cherry tomato fruit. *Microbiol. Spectrum* **2023**, *11* (1), 1−13.

(21) Rinkel, J.; Babczyk, A.; Wang, T.; Stadler, M.; Dickschat, J. S. Volatiles from the hypoxylaceous fungi *Hypoxylon griseobrunneum* and *Hypoxylon macrocarpum*. *Beilstein J. Org. Chem.* **2018**, *14*, 2974−2990.

(22) Al-Toubi, A. S. S.; Al-Sadi, A. M.; Al-Mahmooli, I. H.; Al-Harrasi, M. M. A.; Al Sabahi, J. N.; Velazhahan, R. Volatile organic compounds emitted by mycoparasitic fungi *Hypomyces perniciosus* and *Cladobotryum mycophilum* suppress the growth of *Agaricus bisporus*. *Czech Mycol.* **2022**, *74* (2), 141−152.

(23) Wolfender, J. L.; Gaudry, A.; Rutz, A.; Quiros-Guerrero, L.-M.; Nothias, L.-F.; Queiroz, E. F.; Defossez, E.; Allard, P.-M. Metabolomics in ecology and bioactive natural products discovery: challenges and prospects for a comprehensive study of the specialised metabolome. *Chimia* **2022**, *76* (11), 954−963.

(24) Ntie-Kang, F.; Svozil, D. An enumeration of natural products from microbial, marine and terrestrial sources. *Phys. Sci. Rev.* **2020**, *5* (8), 1−22.

(25) Koutouleas, A.; Collinge, D. B.; Ræbild, A. Alternative plant protection strategies for tomorrow's coffee. *Plant Pathol.* **2023**, *72* (3), 409−429.

(26) Barquero, M. Cafetaleros perdieron 12% de cosecha por lluvia y plagas. La Nación (San José, Costa Rica), December 17, 2010. https://www.nacion.com/economia/cafetaleros-perdieron-12-de-cosecha-por-lluvia-y-plagas/6NKK6NCILRDDXESMW5PN7PURJY/story/ (accessed 2023−04−25).

(27) Avelino, J.; Cabut, S.; Barboza, B.; Barquero, M.; Alfaro, R.; Esquivel, C.; Durand, J.-F.; Cilas, C. Topography and crop management are key factors for the development of American leaf spot epidemics on coffee in Costa Rica. *Phytopathology* **2007**, *97* (2), 1532−1542.

(28) Granados-Montero, M. D. M.; Avelino, J.; Arauz-Cavallini, F.; Castro-Tanzi, S.; Ureña, N. Leaf litter and *Mycena citricolor* inoculum

on the American leaf spot epidemic. *Agron. Mesoamerican* **2020**, *31* (1), 77−94.
(29) Bolívar-Anillo, H. J.; Garrido, C.; Collado, I. G. Endophytic microorganisms for biocontrol of the phytopathogenic fungus *Botrytis cinerea*. *Phytochem. Rev.* **2020**, *19* (3), 721−740.
(30) Syed Ab Rahman, S. F.; Singh, E.; Pieterse, C. M. J.; Schenk, P. M. Emerging microbial biocontrol strategies for plant pathogens. *Plant Sci.* **2018**, *267*, 102−111.
(31) Durham, T. C.; Mizik, T. Comparative economics of conventional, organic, and alternative agricultural production systems. *Economies* **2021**, *9* (2), 64.
(32) Sirikamonsathien, T.; Kenji, M.; Dethoup, T. Potential of endophytic *Trichoderma* in controlling *Phytophthora* leaf fall disease in rubber (*Hevea brasiliensis*). *Biol. Control* **2023**, *179*, No. 105175.
(33) Yang, Y.; Chen, Y.; Cai, J.; Liu, X.; Huang, G. Antifungal activity of volatile compounds generated by endophytic fungi *Sarocladium brachiariae* HND5 against *Fusarium oxysporum* f. sp. *cubense*. *PLoS One* **2021**, *16* (12), No. e0260747.
(34) Escudero-Leyva, E.; Granados-Montero, M. d. D.; Orozco-Ortiz, C.; Araya-Valverde, E.; Alvarado-Picado, E.; Chaves-Fallas, J. M.; Aldrich-Wolfe, L.; Chaverri, P. The endophytobiome of wild Rubiaceae as a source of antagonistic fungi against the American leaf spot of coffee (*Mycena citricolor*). *J. Appl. Microbiol.* **2023**, *134* (5), No. lxad090.
(35) Pujade-Renaud, V.; Déon, M.; Gazis, R.; Ribeiro, S.; Dessailly, F.; Granet, F.; Chaverri, P. Endophytes from wild rubber trees as antagonists of the pathogen *Corynespora cassiicola*. *Phytopathology* **2019**, *109* (11), 1888−1899.
(36) Helaly, S. E.; Thongbai, B.; Stadler, M. Diversity of biologically active secondary metabolites from endophytic and saprotrophic fungi of the ascomycete order Xylariales. *Nat. Prod. Rep.* **2018**, *35* (9), 992−1014.
(37) Stadler, M.; Læssøe, T.; Fournier, J.; Decock, C.; Schmieschek, B.; Tichy, H.-V.; Peršoh, D. A polyphasic taxonomy of *Daldinia* (Xylariaceae). *Stud. Mycol.* **2014**, *77*, 1−143.
(38) Liarzi, O.; Bar, E.; Lewinsohn, E.; Ezra, D. Use of the endophytic fungus *Daldinia* cf. *concentrica* and its volatiles as bio-control agents. *PLoS One* **2016**, *11* (12), No. e0168242.
(39) Khruengsai, S.; Pripdeevech, P.; Tanapichatsakul, C.; Srisuwannapa, C.; D'Souza, P. E.; Panuwet, P. Antifungal properties of volatile organic compounds produced by *Daldinia eschscholtzii* MFLUCC 19−0493 isolated from *Barleria prionitis* leaves against *Colletotrichum acutatum* and its postharvest infections on strawberry fruits. *PeerJ* **2021**, *9*, No. e11242.
(40) Pandey, A.; Banerjee, D. *Daldinia bambusicola* Ch4/11 an endophytic fungus producing volatile organic compounds having antimicrobial and olio chemical potential. *J. Adv. Microbiol.* **2014**, *1* (6), 330−337.
(41) Sanadhya, P.; Bucki, P.; Liarzi, O.; Ezra, D.; Gamliel, A.; Miyara, S. B. *Caenorhabditis elegans* susceptibility to *Daldinia* cf. *concentrica* bioactive volatiles is coupled with expression activation of the stress-response transcription factor daf-16, a part of distinct nematicidal action. *PLoS One* **2018**, *13* (5), No. e0196870.
(42) Macías-Rubalcava, M. L.; Sánchez-Fernández, R. E.; Roque-Flores, G.; Lappe-Oliveras, P.; Medina-Romero, Y. M. Volatile organic compounds from *Hypoxylon anthochroum* endophytic strains as postharvest mycofumigation alternative for cherry tomatoes. *Food Microbiol.* **2018**, *76*, 363−373.
(43) Bejarano, A.; Puopolo, G. Bioformulation of microbial biocontrol agents for a sustainable agriculture. In *How Research Can Stimulate the Development of Commercial Biological Control Against Plant Diseases*; De Cal, A.; Melgarejo, P.; Magan, N., Eds.; Progress in Biological Control; Springer, Nature: Switzerland, 2020; Vol. *21*, pp 275−294. DOI: 10.1007/978-3-030-53238-3_16.
(44) Inamdar, A. A.; Morath, S.; Bennett, J. W. Fungal Volatile Organic Compounds: More than just a funky smell. *Annu. Rev. Microbiol.* **2020**, *74*, 101−116.
(45) Smirnov, A.; Jia, W.; Walker, D. I.; Jones, D. P.; Du, X. ADAP-GC 3.2: Graphical software tool for efficient spectral deconvolution of Gas Chromatography-High-Resolution mass spectrometry metabolomics Data. *J. Proteome Res.* **2018**, *17* (1), 470−478.
(46) Pluskal, T.; Castillo, S.; Villar-Briones, A.; Orešič, M. MZmine 2: Modular framework for processing, visualizing, and analyzing mass spectrometry-based molecular profile data. *BMC Bioinf.* **2010**, *11* (1), No. 395.
(47) Kim, H. W.; Wang, M.; Leber, C. A.; Nothias, L.-F.; Reher, R.; Kang, K. B.; van der Hooft, J. J.; Dorrestein, P. C.; Gerwick, W. H.; Cottrell, G. W. NPClassifier: A deep neural network-based structural classification tool for natural products. *J. Nat. Prod.* **2021**, *84* (11), 2795−2807.
(48) Fiehn, O. Metabolomics by Gas Chromatography-Mass Spectrometry: the combination of targeted and untargeted profiling. *Curr. Protoc. Mol. Biol.* **2016**, *114* (1), 30.4.1−30.4.32.
(49) Lucero, M.; Estell, R.; Tellez, M.; Fredrickson, E. A retention index calculator simplifies identification of plant volatile organic compounds. *Phytochem. Anal.* **2009**, *20* (5), 378−384.
(50) Schymanski, E. L.; Jeon, J.; Gulde, R.; Fenner, K.; Ruff, M.; Singer, H. P.; Hollender, J. Identifying small molecules via high resolution mass spectrometry: Communicating confidence. *Environ. Sci. Technol.* **2014**, *48* (4), 2097−2098.
(51) Goodacre, R.; Broadhurst, D.; Smilde, A. K.; Kristal, B. S.; Baker, J. D.; Beger, R.; Bessant, C.; Connor, S.; Capuani, G.; Craig, A.; Ebbels, T.; Kell, D. B.; Manetti, C.; Newton, J.; Paternostro, G.; Somorjai, R.; Sjöström, M.; Trygg, J.; Wulfert, F. Proposed minimum reporting standards for data analysis in metabolomics. *Metabolomics* **2007**, *3* (3), 231−241.
(52) Wang, T.; Mohr, K. I.; Stadler, M.; Dickschat, J. S. Volatiles from the tropical ascomycete *Daldinia clavata* (Hypoxylaceae, Xylariales). *Beilstein J. Org. Chem.* **2018**, *14*, 135−147.
(53) Tolouee, M.; Alinezhad, S.; Saberi, R.; Eslamifar, A.; Zad, S. J.; Jaimand, K.; Taeb, J.; Rezaee, M.-B.; Kawachi, M.; Shams-Ghahfarokhi, M.; Razzaghi-Abyaneh, M. Effect of *Matricaria chamomilla* L. flower essential oil on the growth and ultrastructure of *Aspergillus niger* van Tieghem. *Int. J. Food Microbiol.* **2010**, *139* (3), 127−133.
(54) Niogret, J.; Kendra, P. E.; Epsky, N. D.; Heath, R. R. Comparative analysis of terpenoid emissions from Florida host trees of the redbay ambrosia beetle, *Xyleborus glabratus* (Coleoptera: Curculionidae: Scolytinae). *Florida Entomol.* **2011**, *94* (4), 1010−1017.
(55) De Alfonso, I.; Vacas, S.; Primo, J. Role of α-copaene in the susceptibility of olive fruits to *Bactrocera oleae* (Rossi). *J. Agric. Food Chem.* **2014**, *62* (49), 11976−11979.
(56) Nishida, R.; Shelly, T. E.; Whittier, T. S.; Kaneshiro, K. Y. α-Copaene, a potential rendezvous cue for the Mediterranean fruit fly, *Ceratitis capitata*. *J. Chem. Ecol.* **2000**, *26* (1), 87−100.
(57) Pathania, A. S.; Guru, S. K.; Ashraf, N. U.; Riyaz-UI-Hassan, S.; Ali, A.; Tasduq, S. A.; Malik, F.; Bhushan, S. A novel stereo bioactive metabolite isolated from an endophytic fungus induces caspase dependent apoptosis and STAT-3 inhibition in human leukemia cells. *Eur. J. Pharmacol.* **2015**, *765*, 75−85.
(58) Flores-Reséndiz, M.; Lappe-Oliveras, P.; Macías-Rubalcava, M. L. Mitochondrial damage produced by phytotoxic chromenone and chromanone derivatives from endophytic fungus *Daldinia eschscholtzii* strain GsE13. *Appl. Microbiol. Biotechnol.* **2021**, *105* (10), 4225−4239.
(59) Musteata, F. M.; Vuckovic, D. *In Vivo* Sampling with Solid-Phase Microextraction. In *Handbook of Solid Phase Microextraction*; Elsevier, 2012; pp 399−453. DOI: 10.1016/B978-0-12-416017-0.00012-7.
(60) Molinski, T. F. NMR of natural products at the 'nanomole-scale'. *Nat. Prod. Rep.* **2010**, *27* (3), 321−329.
(61) Cuesta-Rubio, O.; Piccinelli, A. L.; Fernandez, M. C.; Hernández, I. M.; Rosado, A.; Rastrelli, L. Chemical characterization of Cuban propolis by HPLC-PDA, HPLC-MS, and NMR: The brown, red, and yellow Cuban varieties of propolis. *J. Agric. Food Chem.* **2007**, *55* (18), 7502−7509.
(62) Dai, J.; Krohn, K.; Flörke, U.; Draeger, S.; Schulz, B.; Kiss-Szikszа, A.; Antus, S.; Kurtán, T.; van Ree, T. Metabolites from the endophytic fungus *Nodulisporium* sp. from *Juniperus cedre*. *Eur. J. Org. Chem.* **2006**, *2006*, 3498−3506.

(63) Kongyen, W.; Rukachaisirikul, V.; Phongpaichit, S.; Sakayaroj, J. A new hydronaphthalenone from the mangrove-derived *Daldinia eschscholtzii* PSU-STD57. *Nat. Prod. Res.* **2015**, *29* (21), 1995−1999.
(64) Yang, L.-J.; Liao, H.-X.; Bai, M.; Huang, G.-L.; Luo, Y.-P.; Niu, Y.-Y.; Zheng, C.-J.; Wang, C.-Y. One new cytochalasin metabolite isolated from a mangrove-derived fungus *Daldinia eschscholtzii* HJ001. *Nat. Prod. Res.* **2018**, *32* (2), 208−213.
(65) Chang, C. W.; Chang, H.-S.; Cheng, M.-J.; Liu, T.-W.; Hsieh, S.-Y.; Yuan, G.-F.; Chen, I.-S. Inhibitory effects of constituents of an endophytic fungus *Hypoxylon investiens* on nitric oxide and interleukin-6 production in RAW264.7 macrophages. *Chem. Biodivers.* **2014**, *11* (6), 949−961.
(66) Bajpai, V. K.; Shukla, S.; Kang, S. C. Chemical composition and antifungal activity of essential oil and various extract of *Silene armeria* L. *Bioresour. Technol.* **2008**, *99* (18), 8903−8908.
(67) Geng, Y.; Gui, K.; Pan, T.; Ye, J.; Li, J.; Feng, J.; Ma, Z.; Lei, P.; Gao, Y. Preparation of terpene-derived fungicidal candidates with a 1,3,4-thiadiazole moiety for natural product-inspired agrochemical discovery. *Ind. Crops Prod.* **2022**, *189*, No. 115889.
(68) Souza, D. P.; Pimentel, R. B. Q.; Santos, A.; Albuquerque, P. M.; Fernandes, A. V.; Junior, S. D.; Oliveira, J. T. A.; Ramos, M. V.; Rathinasabapathi, B.; Gonçalves, J. F. C. Fungicidal properties and insights on the mechanisms of the action of volatile oils from Amazonian Aniba trees. *Ind. Crops Prod.* **2020**, *143*, No. 111914.
(69) Zhang, J.; Tian, H.; Sun, H.; Wang, X. Antifungal activity of trans-2-hexenal against *Penicillium cyclopium* by a membrane damage mechanism. *J. Food Biochem.* **2017**, *41* (2), No. e12289.
(70) Li, S. F.; Zhang, S.-B.; Zhai, H.-C.; Lv, Y.-Y.; Hu, Y.-S.; Cai, J.-P. Hexanal induces early apoptosis of *Aspergillus flavus* conidia by disrupting mitochondrial function and expression of key genes. *Appl. Microbiol. Biotechnol.* **2021**, *105* (18), 6871−6886.
(71) Schmid, R.; Heuckeroth, S.; Korf, A.; et al. Integrative analysis of multimodal mass spectrometry data in MZmine 3. *Nat. Biotechnol.* **2023**, *41* (4), 447−449.
(72) Wang, M.; Carver, J. J.; Phelan, V.; et al. Sharing and community curation of mass spectrometry data with Global Natural Products Social Molecular Networking. *Nat. Biotechnol.* **2016**, *34* (8), 828−837.
(73) Dührkop, K.; Fleischauer, M.; Ludwig, M.; Aksenov, A. A.; Melnik, A. V.; Meusel, M.; Dorrestein, P. C.; Rousu, J.; Böcker, S. SIRIUS 4: a rapid tool for turning tandem mass spectra into metabolite structure information. *Nat. Methods* **2019**, *16* (4), 299−302.
(74) Quiros-Guerrero, L. M.; Nothias, L.-F.; Gaudry, A.; Marcourt, L.; Allard, P.-M.; Rutz, A.; David, B.; Queiroz, E. F.; Wolfender, J.-L. Inventa: A computational tool to discover structural novelty in natural extracts libraries. *Front. Mol. Biosci.* **2022**, *9*, No. 1028334.
(75) Dührkop, K.; Nothias, L.-F.; Fleischauer, M.; Reher, R.; Ludwig, M.; Hoffmann, M.; Petras, D.; Gerwick, W. H.; Rousu, J.; Dorrestein, P. C.; Böcker, S. Systematic classification of unknown metabolites using high-resolution fragmentation mass spectra. *Nat. Biotechnol.* **2021**, *39* (4), 462−471.
(76) Schmid, R.; Petras, D.; Nothias, L.-F.; et al. Ion identity molecular networking for mass spectrometry-based metabolomics in the GNPS environment. *Nat. Commun.* **2021**, *12* (1), No. 3832.
(77) Theodoridis, G.; Gika, H.; Raftery, D.; Goodacre, R.; Plumb, R. S.; Wilson, I. D. Ensuring fact-based metabolite identification in liquid chromatography-mass spectrometry-based metabolomics. *Anal. Chem.* **2023**, *95* (8), 3909−3916.
(78) Hanson, B. J. R. Fungi and the development of microbiological chemistry. In *The Chemistry of Fungi*; Royal Society of Chemistry: Cambridge, 2008; pp 6−15.
(79) Thevissen, K.; Ferket, K. K. A.; François, I. E. J. A.; Cammue, B. P. A. Interactions of antifungal plant defensins with fungal membrane components. *Peptides* **2003**, *24* (11), 1705−1712.
(80) Lohmann, J. S.; Wagner, S.; von Nussbaum, M.; Pulte, A.; Steglich, W.; Spiteller, P. Mycenaflavin A, B, C, and D: Pyrroloquinoline alkaloids from the fruiting bodies of the mushroom *Mycena haematopus*. *Chem. − Eur. J.* **2018**, *24* (34), 8609−8614.
(81) Peters, S.; Spiteller, P. Mycenarubins A and B, red pyrroloquinoline alkaloids from the mushroom *Mycena rosea*. *Eur. J. Org. Chem.* **2007**, *2007*, 1571−1576.
(82) Isaka, M.; Chinthanom, P.; Sappan, M.; Supothina, S.; Boonpratuang, T. Phenylglycol metabolites from cultures of the basidiomycete *Mycena pruinosoviscida* BCC 22723. *Helv. Chim. Acta* **2014**, *97* (7), 909−914.
(83) Azzollini, A.; Boggia, L.; Boccard, J.; Sgorbini, B.; Lecoultre, N.; Allard, P.-M.; Rubiolo, P.; Rudaz, S.; Gindro, K.; Bicchi, C.; Wolfender, J.-C. Dynamics of metabolite induction in fungal co-cultures by metabolomics at both volatile and non-volatile levels. *Front. Microbiol.* **2018**, *9*, 72.
(84) Rai, M.; Agarkar, G. Plant-fungal interactions: What triggers the fungi to switch among lifestyles? *Crit. Rev. Microbiol.* **2016**, *42* (3), 428−438.
(85) Arnold, A. E.; Mejia, L. C.; Kyllo, D.; Rojas, E. I.; Maynard, Z.; Robbins, N.; Herre, E. A. Fungal endophytes limit pathogen damage in a tropical tree. *Proc. Natl. Acad. Sci. U.S.A.* **2003**, *100* (26), 15649−15654.
(86) Chambers, M. C.; Maclean, B.; Burke, R.; et al. A cross-platform toolkit for mass spectrometry and proteomics. *Nat. Biotechnol.* **2012**, *30* (10), 918−920.
(87) Aron, A. T.; Gentry, E.; McPhail, K. L.; Nothias, L.-F.; Nothias-Esposito, M.; Bouslimani, A.; et al. Reproducible molecular networking of untargeted mass spectrometry data using GNPS. *Nat. Protoc.* **2020**, *15* (6), 1954−1991.
(88) R Core Team. *R: A language and environment for statistical computing*, 2020 https://www.r-project.org/ (accessed 2023−01−10).
(89) Lê, S.; Josse, J.; Husson, F. FactoMineR: An R package for multivariate analysis. *J. Stat. Software* **2008**, *25* (1), 1−18.
(90) Kassambara, A.; Mundt, F. *Release 2020: Factoextra: extract and visualize the results of multivariate data analyses*. R package version 1.0.7, 2020. https://CRAN.R-project.org/package=factoextra (accessed 2023−04−15).
(91) Rohart, F.; Gautier, B.; Singh, A.; Lê Cao, K. A. mixOmics: An R package for 'omics feature selection and multiple data integration. *PLoS Comput. Biol.* **2017**, *13* (11), No. e1005752.
(92) Bertrand, S.; Schumpp, O.; Bohni, N.; Bujard, A.; Azzollini, A.; Monod, M.; Gindro, K.; Wolfender, J.-L. Detection of metabolite induction in fungal co-cultures on solid media by high-throughput differential ultra-high pressure liquid chromatography-time-of-flight mass spectrometry fingerprinting. *J. Chromatogr. A* **2013**, *1292*, 219−228.
(93) Ludwig, M.; Nothias, L.-F.; Dührkop, K.; et al. Database-independent molecular formula annotation using Gibbs sampling through ZODIAC. *Nat. Mach. Intell.* **2020**, *2* (10), 629−641.
(94) Dührkop, K.; Shen, H.; Meusel, M.; Rousu, J.; Böcker, S. Searching molecular structure databases with tandem mass spectra using CSI:FingerID. *Proc. Natl. Acad. Sci. U.S.A.* **2015**, *112* (41), 12580−12585.
(95) Hoffmann, M. A.; Nothias, L.-F.; Ludwig, M.; Fleischauer, M.; Gentry, E. C.; Witting, M.; Dorrestein, P. C.; Dührkop, K.; Böcker, S. High-confidence structural annotation of metabolites absent from spectral libraries. *Nat. Biotechnol.* **2022**, *40* (3), 411−421.

https://doi.org/10.1021/acsomega.3c03865
ACS Omega 2023, 8, 31373−31388